Supporting Information for the paper entitled,

A Super-Oxidized Radical Cationic Icosahedral Boron Cluster

Julia M. Stauber,[1] Josef Schwan,[2] Xinglong Zhang,[2] Jonathan C. Axtell,[1,3] Dahee Jung,[1] Brendon J. McNicholas,[2] Paul H. Oyala,[2] Andrew J. Martinolich,[2] Jay R. Winkler,[2] Kimberly A. See,[2] Thomas F. Miller III,[2]* Harry B. Gray,[2]* Alexander M. Spokoyny[1,4]*

[1]*Department of Chemistry and Biochemistry, University of California, Los Angeles, 607 Charles E. Young Dr E., Los Angeles, California, 90095, United States*

[2]*Division of Chemistry and Chemical Engineering, California Institute of Technology, 1200 East California Boulevard, Pasadena, California, 91125, United States*

[3]*The Dow Chemical Company, 633 Washington St., Midland, Michigan, 48674, United States*

[4]*California NanoSystems Institute, University of California, Los Angeles, 570 Westwood Plaza, Los Angeles, California, 90095, United States*

*Correspondence to: spokoyny@chem.ucla.edu (A. M. S.), hbgray@caltech.edu (H. B. G.), tfm@caltech.edu (T. F. M.)

Contents

S1. General considerations

S1.1. Materials

All manipulations were performed under an inert atmosphere of purified N_2 in a Vacuum Atmospheres NexGen glovebox unless otherwise indicated. All reagents were purchased from Sigma Aldrich, Oakwood Chemicals, TCI, Fisher Scientific, or Alfa Aesar, and used as received unless otherwise noted. Dichloromethane (DCM), tetrahydrofuran (THF), toluene, and diethyl ether (Et_2O) were purified on a JC Meyer Glass Contour Solvent Purification System and stored under argon prior to use. All other solvents were used as received without further purification unless otherwise specified (acetone, acetonitrile (MeCN), ethyl acetate (EtOAc), hexanes). [TBA][PF_6] was purchased from Sigma Aldrich and recrystallized three times from hot EtOH and dried under dynamic vacuum at 80 °C for 12 h prior to use. $[TBA]_2[B_{12}(OH)_{12}]$ was prepared following previously reported procedures,[1] and was stored under an atmosphere of purified N_2 in a Vacuum Atmospheres NexGen glovebox prior to use. $[N(2,4\text{-}Br_2C_6H_3)_3][SbCl_6]$ was prepared according to a reported procedure,[2] and was stored under an inert atmosphere of N_2 at -30 °C. Deuterated solvents (C_6D_6, $CDCl_3$, THF-d_8) were obtained from Cambridge Isotope Laboratories and degassed and stored over molecular sieves (4 Å beads) for at least two days prior to use. Celite was dried by heating above 200 °C under dynamic vacuum for at least 24 h prior to use. Molecular sieves (4 Å beads, 8-12 mesh) were activated by heating above 250 °C under dynamic vacuum for at least 24 h prior to use.

S1.2. Methods

All NMR spectra were obtained on Bruker Avance 400 or 300 MHz broad band FT NMR spectrometers. ^{1}H NMR and $^{13}C\{^1H\}$ NMR spectra were referenced to residual protio-solvent signals, and $^{11}B\{^1H\}$ chemical shifts were referenced to BF_3•Et_2O (15% in $CDCl_3$, δ 0.0 ppm). ESI-MS data were collected on a Thermo Instruments Q-Exactive Plus Hybrid Quadrupole-Orbitrap instrument operating in ESI-positive mode. Full mass scan (500 to 4000 *m/z*) was used at 70,000 resolution, with automatic gain control (AGC) target of 1 x 10^6 ions, electrospray ionization operating at a 1.5 kV spray voltage, and a capillary temperature of 250 °C. X-band continuous wave EPR measurements were carried out using a Bruker EMX spectrometer at 77K with a microwave frequency of 9.3468 GHz, and the data were acquired using Bruker Win-EPR software (ver. 3.0). UV-vis measurements were conducted using an Ocean Optics Flame-S-UV-VIS-ES miniature spectrometer equipped with a DH-2000 UV-vis NIR light source. All measurements were carried out using quartz cuvettes (1 cm path length) and conducted at 25 °C with solution samples at the indicated concentrations. Cyclic voltammetry measurements were performed with a Gamry Instruments Interface 1010E potentiostat using a glassy carbon disc working electrode, platinum wire counter electrode and a Ag wire pseudo-reference electrode. Measurements were conducted with [TBA][PF_6] (0.1 M, DCM) supporting electrolyte in dry DCM under an inert atmosphere of purified N_2 and referenced *vs.* Fc/Fc^+.

Microwave reactions were performed using a CEM® Discover SP microwave synthesis reactor. All reactions were performed in 35 mL Pyrex microwave pressure vessels purchased from CEM with silicone/PTFE caps. Teflon coated stir bars were used in the vessels with magnetic stirring set to high with 15 s of premixing prior to temperature ramping. All microwave reactions were carried out at 140 °C with the pressure release limit set to 250 psi and the maximum wattage set to 250 W. The power applied was dynamically controlled by the microwave instrument and did not exceed this limit for any reactions.

S2. Synthetic procedures and characterization data for all compounds

S2.1. B_{12}(O-3-methylbutyl)$_{12}$ (1)

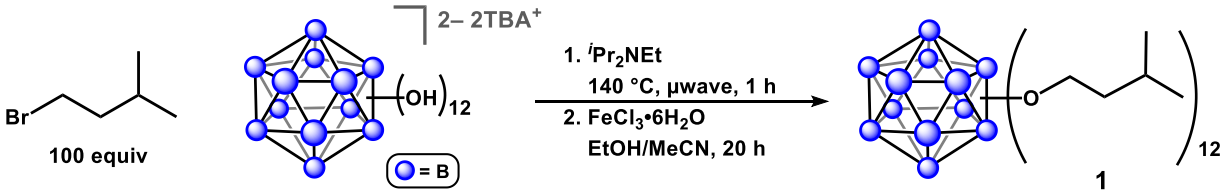

The B_{12}(O-3-methylbutyl)$_{12}$ (**1**) cluster was originally reported by Hawthorne *et al*.[3] Provided below is a modified protocol employing a microwave-assisted synthetic procedure[1] that reduced the alkylation reaction time from the reported 8 h to 1 h. The characterization data of **1** collected following this procedure are also provided and agree well with reported data.[3]

Tetrabutylammonium is defined as $[^{n}Bu_4N]^+$, and will be referred to as [TBA] throughout the Supporting Information.

$[TBA]_2[B_{12}(OH)_{12}]$ (300 mg, 0.366 mmol, 1.00 equiv) was removed from a nitrogen-filled glovebox and transferred to a 35 mL microwave pressure vessel open to air and equipped with a Teflon-coated stir bar. To this tube was added 1-bromo-3-methylbutane (4.39 mL, 36.6 mmol, 100 equiv) and *N*,*N*-diisopropylethylamine (1.21 mL, 6.95 mmol, 19.0 equiv), followed by MeCN (1 mL). The reaction tube was capped with a PTFE/silicone cap and the mixture was heated to 140 °C with stirring in the microwave for 1 h. The reaction mixture was then removed from the microwave, and the resulting bright magenta reaction mixture was evaporated to dryness to remove unreacted 1-bromo-3-methylbutane. The residue was then suspended in hexanes (4 mL) and loaded into a silica-packed column. The neutral **1** cluster was eluted first with hexanes, followed by elution of a mixture of [TBA][**1**] and $[TBA]_2$[**1**] as a bright magenta band with acetone. The hexane and acetone solutions were evaporated to dryness and then the [TBA][**1**]/$[TBA]_2$[**1**] mixture was suspended in 90:10 EtOH:MeCN (5 mL). To this suspension was added $FeCl_3$•$6H_2O$ (900 mg, 3.33 mmol, 9.10 equiv) as a solid, and the suspension was allowed to stir at 25 °C for a total of 20 h, at which point all volatiles were removed *in vacuo*. The resulting dark brown residue was suspended in hexane (4 mL) and the bright yellow, neutral **1** product was eluted through a silica plug with hexanes. The yellow solution was collected, combined with the fraction containing the neutral **1** cluster recovered from the previous step, and all volatiles were removed under reduced pressure. The brown/orange residue was dissolved in hexanes (1 mL), and MeCN (50 mL) was added with vigorous stirring to precipitate the neutral **1** product from solution as an orange solid, which was collected by filtration and dried under reduced pressure (yield: 224 mg, 0.191 mmol, 52%). ^{1}H NMR (400 MHz, 25 °C, $CDCl_3$) δ: 4.05 (t, 24H, O–CH_2–CH_2, ^3J = 7 Hz), 1.72 (sep, 12H, CH, ^3J = 7 Hz), 1.43 (q, 24H, CH_2–CH_2–CH,^3J = 7 Hz), 0.88 (d, 72H, CH_3, ^3J = 7 Hz) ppm. ^{11}B{^{1}H} NMR (128 MHz, 25 °C, $CDCl_3$) δ: 41.4 ppm. UV-vis (DCM, 25 °C, 80 μM) [Ɛ]: λ_{max} 466 nm [13,000 $M^{-1}cm^{-1}$]. ESI-MS(+) (MeCN) $[M+Na]^+$: 1198.0810 (calc'd, 1198.0838) *m/z.* This species is observed as the $[M+Na]^+$ adduct under ESI-MS(+) conditions.

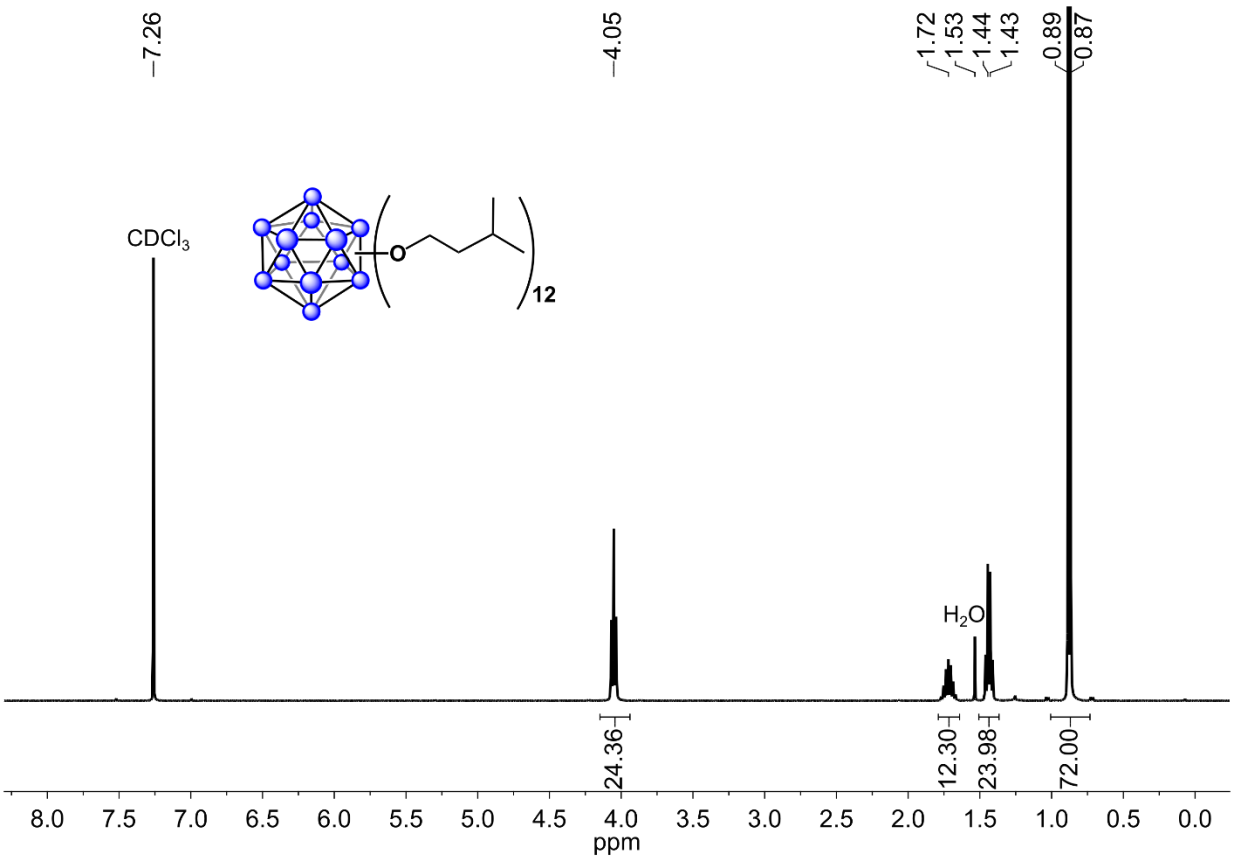

Figure S1. ^{1}H NMR spectrum of **1** ($CDCl_3$, 400 MHz, 25 °C).

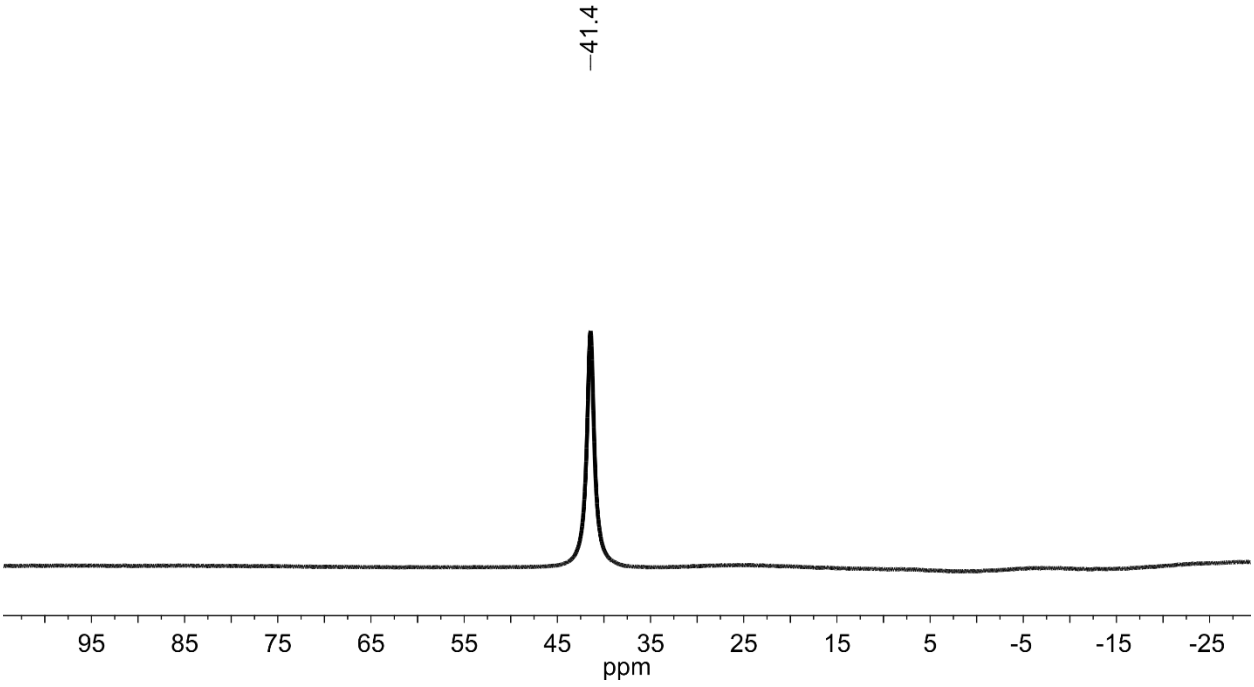

Figure S2. $^{11}B\{^{1}H\}$ NMR spectrum of **1** ($CDCl_3$, 128 MHz, 25 °C).

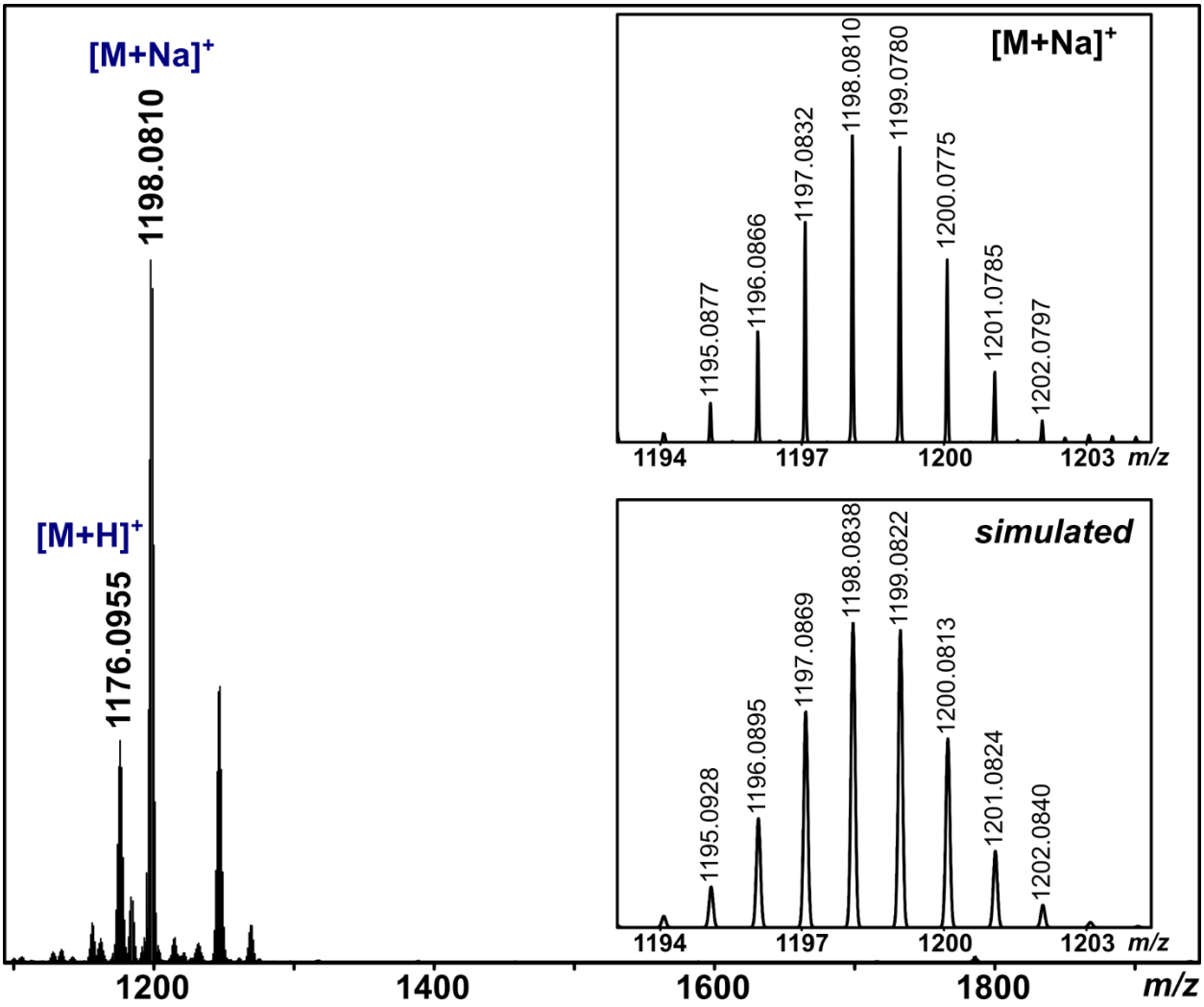

Figure S3. ESI-MS(+) of **1** (MeCN, 1.5 kV). This species is observed as the $[M+H]^+$ (1176.0955 *m/z*) and $[M+Na]^+$ (1198.0810 *m/z*) adducts under ESI-MS conditions.

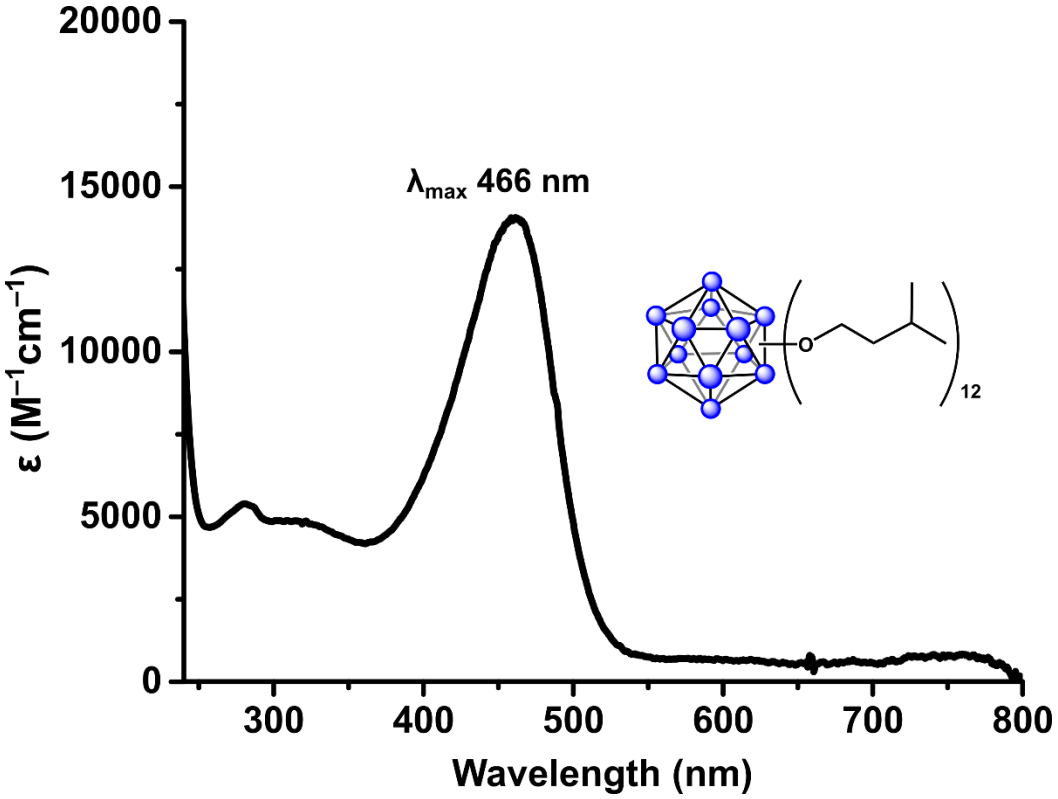

Figure S4. UV-vis spectrum of **1** (DCM, 80 µM, 25 °C).

S2.2. $[Na(Et_2O)]_2[B_{12}(O\text{-}3\text{-}methylbutyl)_{12}]$ ($[Na(Et_2O)]_2$[1])

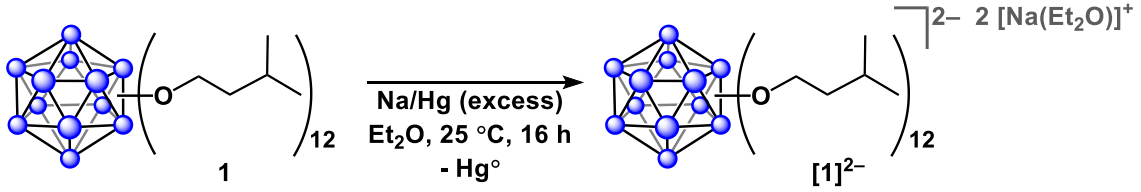

In the glovebox, Na/Hg amalgam (Sigma Aldrich beads, 10% Na, 280 mg, >100 equiv Na) was added to a dark yellow, vigorously stirring solution of **1** (20 mg, 0.017 mmol, 1.0 equiv) in Et_2O (2 mL). The reaction mixture was allowed to stir at glovebox temperature for 16 h, during which time the solution gradually became bright pink and then colorless. The reaction mixture was then filtered through a pad of Celite, and the colorless filtrate was evaporated to dryness to afford $[Na(Et_2O)]_2$[**1**] as a colorless solid (18 mg, 0.013 mmol, 77%). ^{1}H NMR (400 MHz, 25 °C, C_6D_6) δ: 4.42 (t, 24H, O–C*H*$_2$–CH$_2$, ^3J = 7 Hz), 3.26 (q, 4H, Et_2O), 1.99 (sep, 12H, C*H*, ^3J = 7 Hz), 1.72 (q, 24H, CH$_2$–C*H*$_2$–CH, ^3J = 7 Hz), 1.18 (d, 72H, C*H*$_3$, ^3J = 7 Hz), 1.11 (t, 6H, Et_2O) ppm. ^{11}B{^{1}H} NMR (128 MHz, 25 °C, C_6D_6) δ: -16.4 ppm.

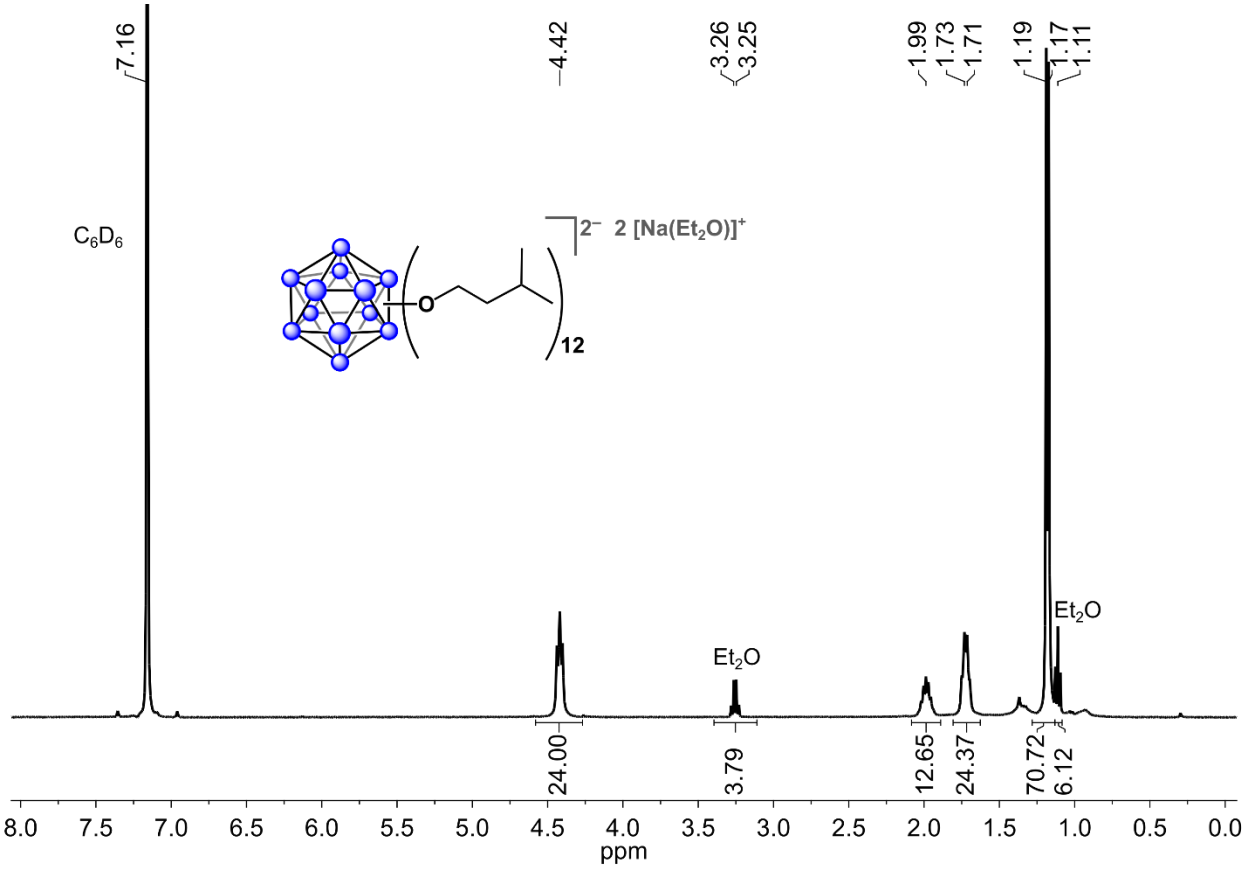

Figure S5. ^{1}H NMR spectrum of $[Na(Et_2O)]_2$[**1**] (C_6D_6, 400 MHz, 25 °C).

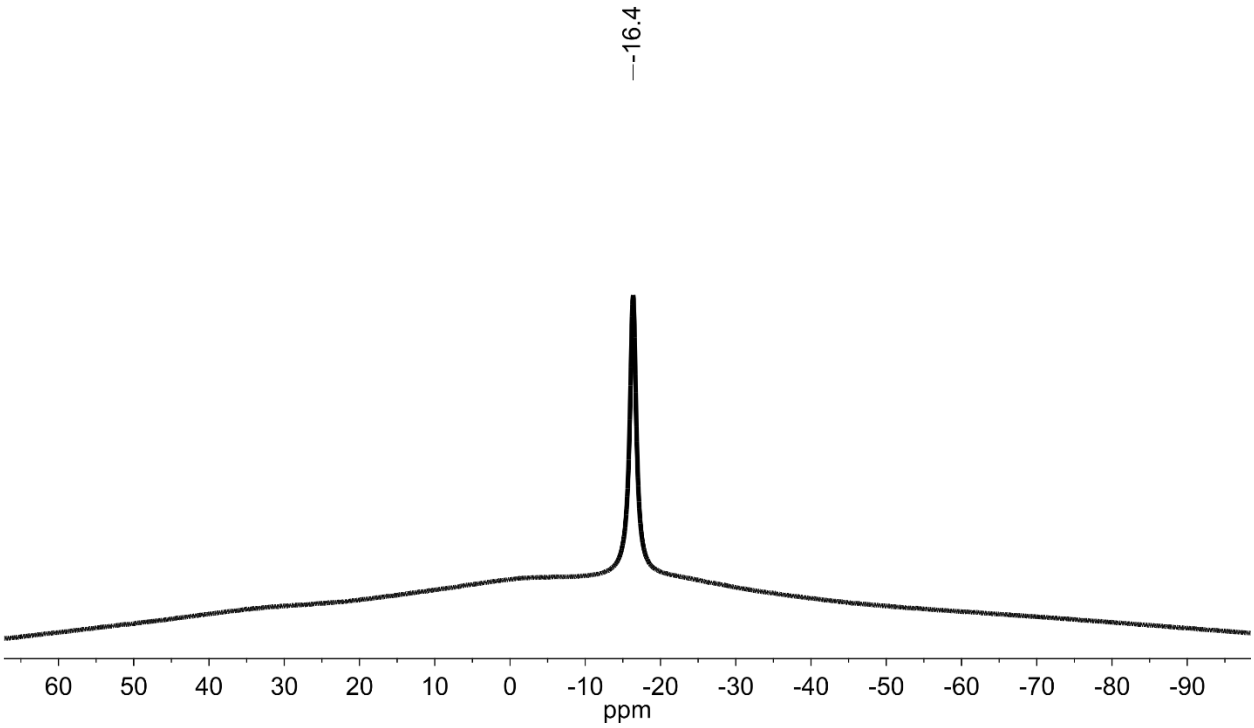

Figure S6. $^{11}B\{^{1}H\}$ NMR spectrum of $[Na(Et_2O)]_2$[**1**] (C_6D_6, 128 MHz, 25 °C).

S2.3. [B_{12}(O-3-methylbutyl)][$SbCl_6$] ([1][$SbCl_6$])

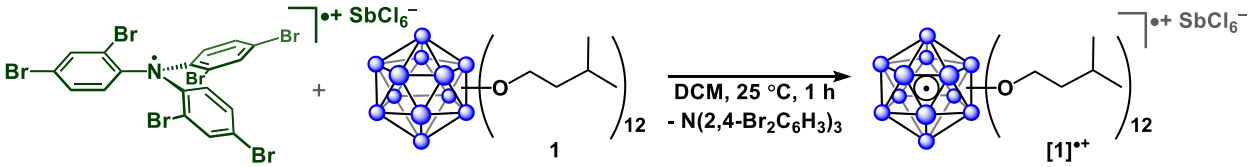

To a dark yellow solution of **1** (15 mg, 0.013 mmol, 1.0 equiv) in DCM (1 mL) was added a green solution of [$N(2,4\text{-}Br_2C_6H_3)_3$][$SbCl_6$] (20 mg, 0.019 mmol, 1.5 equiv) in DCM (1 mL) dropwise over 5 min, during which time the color of the reaction mixture darkened to yellow brown. The reaction mixture was allowed to stir at glovebox temperature for 1 h, at which point all volatiles were removed under reduced pressure. The resulting residue was suspended in pentane (2 mL), stirred for 5 min, and then the pentane was decanted and the residue was dried under reduced pressure to afford [**1**][$SbCl_6$] as a waxy yellow-brown solid (17 mg, 0.011 mmol, 87%). ^{1}H and ^{11}B{^{1}H} NMR spectra were collected immediately, and all subsequent characterization was performed within 24 h after synthesis due to decomposition of the product even when stored under N_2 at -35 °C. ^{1}H NMR (400 MHz, 25 °C, $CDCl_3$) δ: The O–C*H*$_2$–CH_2 resonance is paramagnetically broadened and is therefore not observed due to its proximity to the paramagnetic B_{12} core, 3.38 (br s, 12H, C*H*), 1.76 (br s, 24H, CH_2–C*H*$_2$–CH overlapping with C*H*$_3$ resonance), 1.46 (br s, 72H, C*H*$_3$ overlapping with CH_2–C*H*$_2$–CH resonance) ppm. ^{11}B{^{1}H} NMR (128 MHz, 25 °C, $CDCl_3$) δ: A silent NMR spectrum was observed due to paramagnetic broadening of the ^{11}B NMR signal, which suggests the spin density is delocalized throughout the B_{12} core. UV-vis (DCM, 25 °C, 70 μM) [Ɛ]: λ_{max} 464 (17,000 $M^{-1}cm^{-1}$), 720 (3,000 $M^{-1}cm^{-1}$) nm.

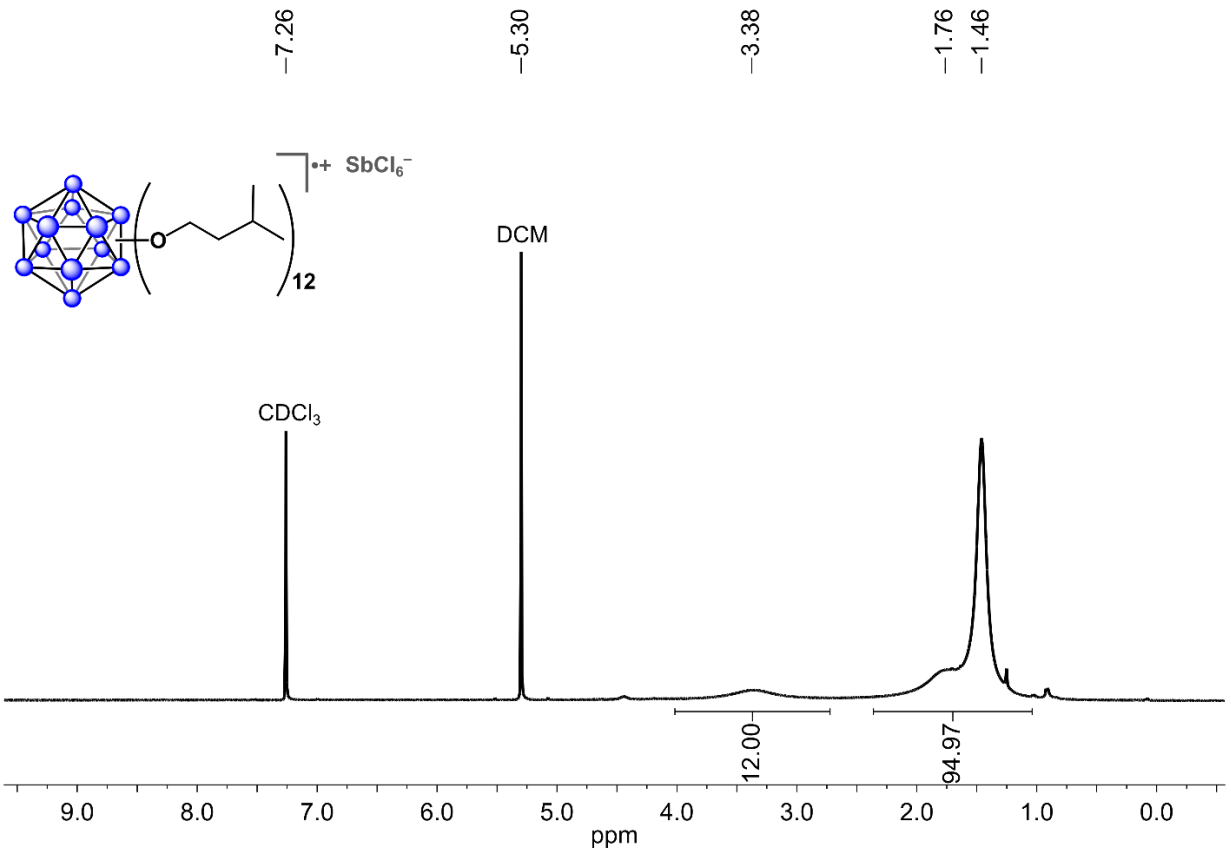

Figure S7. ^{1}H NMR spectrum of [**1**][$SbCl_6$] ($CDCl_3$, 400 MHz, 25 °C).

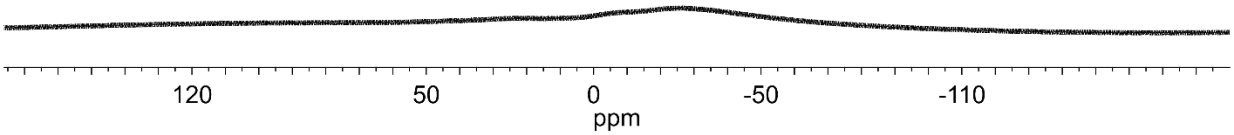

Figure S8. $^{11}B\{^{1}H\}$ NMR spectrum of [**1**][$SbCl_6$] ($CDCl_3$, 128 MHz, 25 °C).

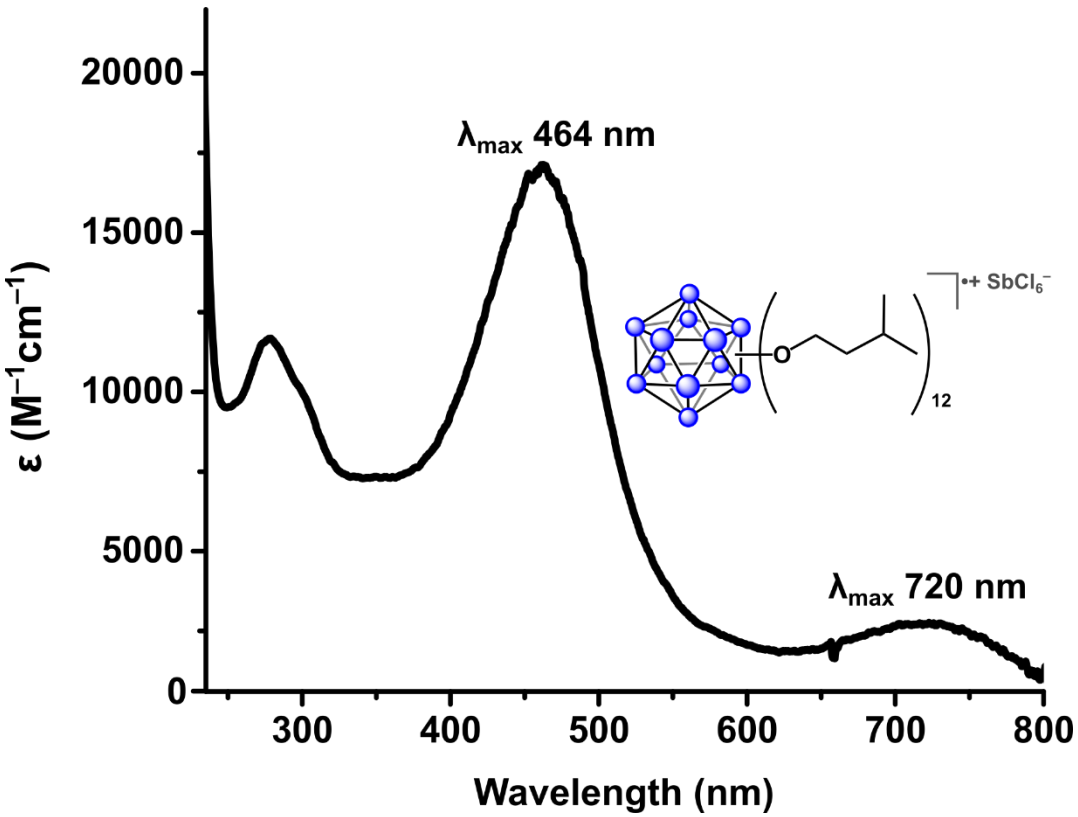

Figure S9. UV-vis spectrum of [**1**][$SbCl_6$] (DCM, 70 µM, 25 °C).

S3. Electrochemical measurements of 1

S3.1. Cyclic voltammetry of 1

Electrochemical measurements of **1** (3 mM solution in DCM) were performed under an inert atmosphere of purified N_2 and referenced *vs.* Fc/Fc^+ (glassy carbon working electrode, Pt wire counter electrode, Ag wire pseudo-reference electrode).

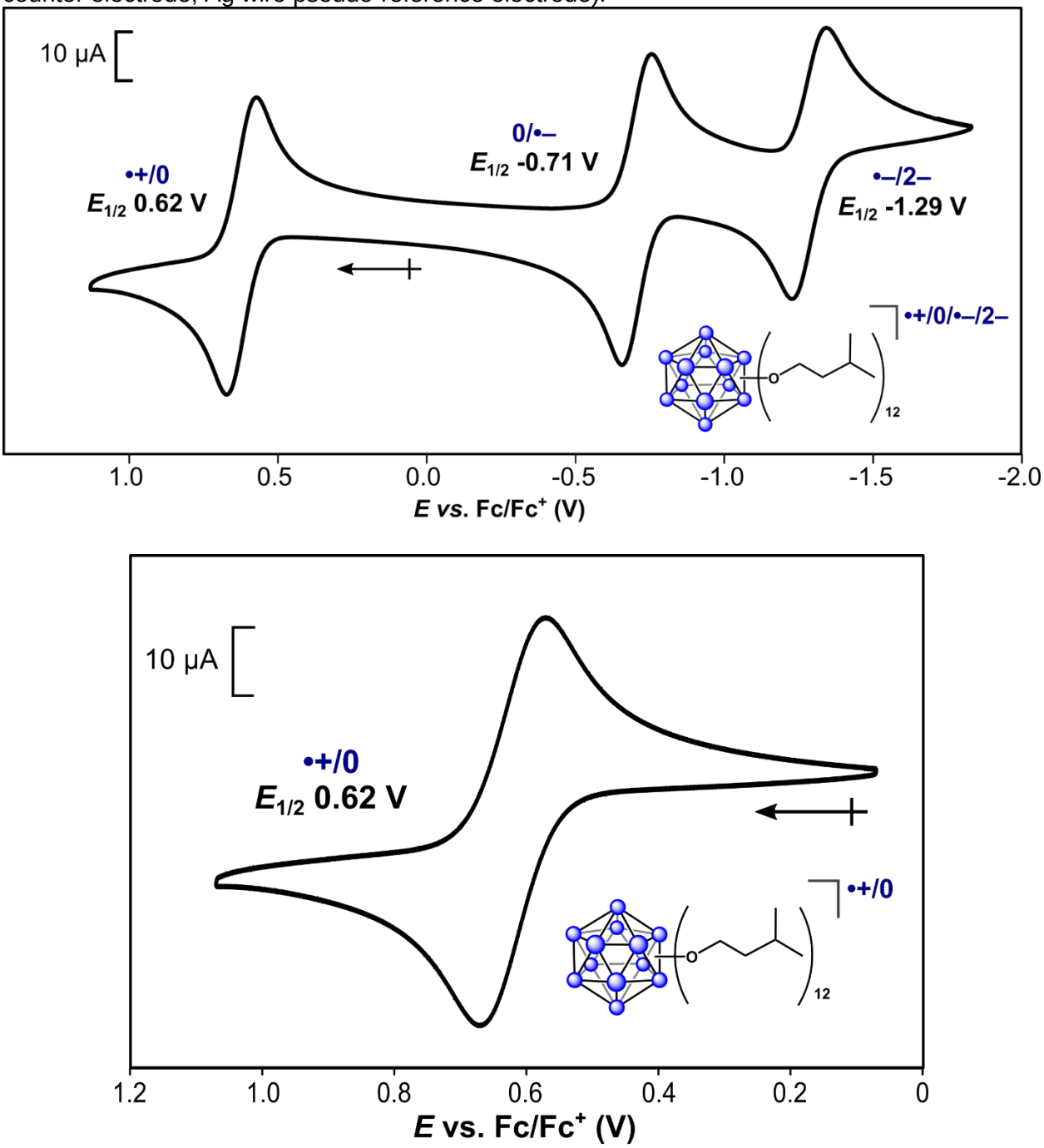

Figure S10. Cyclic voltammogram of **1** measured at a scan rate of 100 mV/s with 0.1 M [TBA][PF_6] supporting electrolyte and referenced *vs*. Fc/Fc^+ (glassy carbon working electrode, platinum counter electrode and Ag wire pseudo-reference electrode; DCM, 3 mM, 25 °C).

S3.2. Randles-Sevcik analysis of the [1]$^{0/\bullet+}$ redox couple

Electrochemical measurements of **1** (3 mM solution in DCM) were performed under an inert atmosphere of purified N_2.Scans were collected between 25-300 mV/s with [TBA][PF_6] supporting electrolyte (0.1 M solution in DCM) and referenced *vs.* Fc/Fc$^+$ (glassy carbon working electrode, Pt wire counter electrode, Ag wire pseudo-reference electrode). The diffusion coefficient (D_0) was calculated according to the Randles-Sevcik equation as described below.[4] The plot of i_p vs. $v^{1/2}$ is linear, as shown below (right), indicating that the electron transfer for the [**1**]$^{0/\bullet+}$ redox event is diffusion controlled.

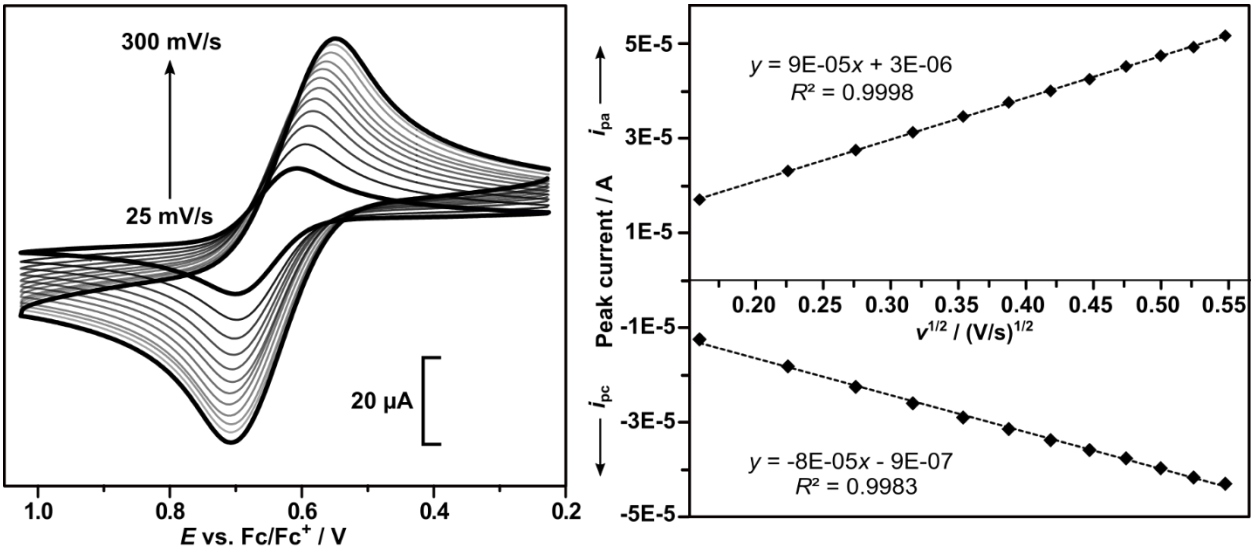

n = number of electrons
F = Faraday's constant
D_0 = diffusion coefficient (cm^2 s^{-1})
v = scan rate (V s^{-1})
A = surface area of the electrode (A = 0.0707 cm^2)
C_0 = bulk concentration of redox-active species (mol cm^{-3})
i_p = peak current

$$i_p = 0.4463 n^{3/2} F^{3/2} A C_0 \sqrt{\frac{D_0 v}{RT}}$$

$$\boldsymbol{D_0 = 3.0 \pm 0.3 \times 10^{-6}\ cm^2\ s^{-1}}$$

Figure S11. (Left) CV of the [**1**]$^{0/\bullet+}$ redox couple recorded at variable scan rates (25-300 mV/s). (Right) Randles-Sevcik plot of the CV data.

S4. X-ray photoelectron spectroscopy data of [1][$SbCl_6$], 1, and [$Na(Et_2O)]_2$[1]

XPS was performed using an AXIS Ultra DLD instrument (Kratos Analytical). All XPS spectra were measured using a monochromatic Al Kα X-ray source (10 mA for both survey and high-resolution scans, 15 kV) with a 300 × 700 nm oval spot size. The pressure of the analyzer chamber was maintained below 5×10^{-8} Torr during the measurement. Spectra were collected with 160 eV pass energy for the survey spectra and 20 eV for high-resolution spectra of O 1*s* and B 1*s* using a 200 ms dwell time. All XPS peaks were charge referenced to the adventitious carbon 1*s* signal at 284.6 eV.

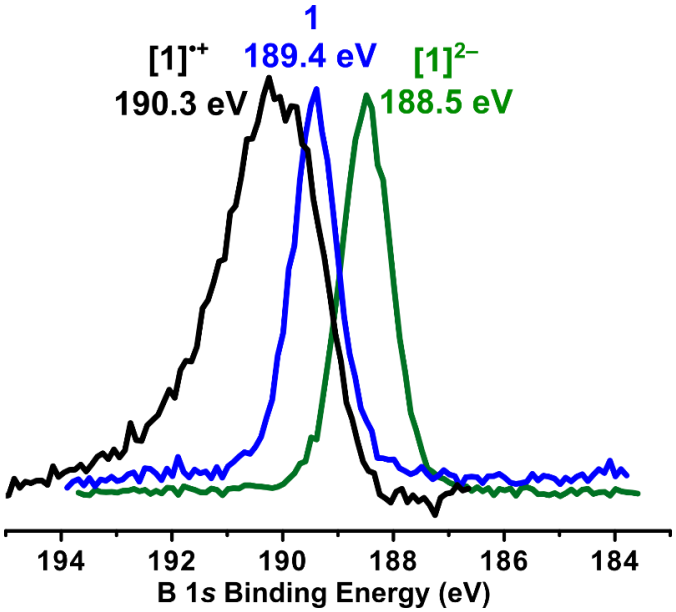

Figure S12. Boron 1*s* X-ray photoelectron spectra of [**1**][$SbCl_6$] (**black**), **1** (**blue**) and [$Na(Et_2O)]_2$[**1**] (**green**).

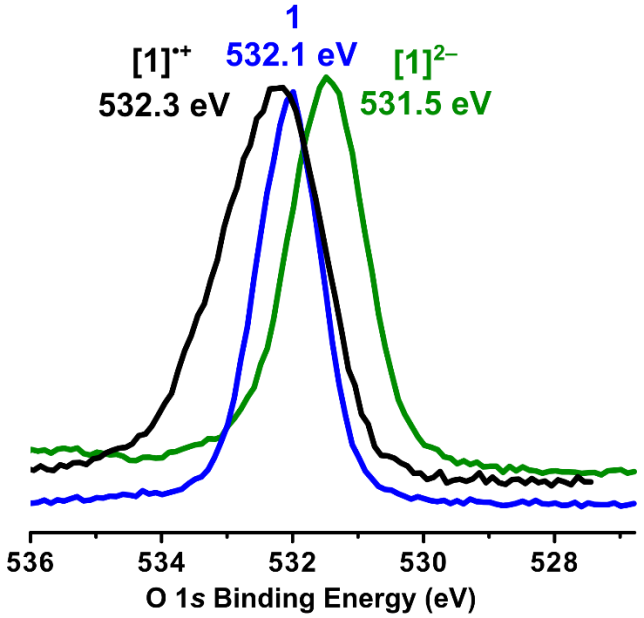

Figure S13. Oxygen 1*s* X-ray photoelectron spectra of [**1**][$SbCl_6$] (**black**), **1** (**blue**) and [$Na(Et_2O)]_2$[**1**] (**green**).

S5. EPR data of [1][$SbCl_6$]

All manipulations were carried out inside a nitrogen-filled glove box. The sample was prepared by dissolution of [$N(2,4\text{-}Br_2C_6H_3)_3$][$SbCl_6$] (2 mg, 0.002 mmol, 0.7 equiv) and **1** (3 mg, 0.003 mg, 1 equiv) in toluene (1 mL). An aliquot of this solution was transferred to an X-band EPR tube equipped with a J. Young valve, which was immediately sealed, removed from the glove box and frozen in liquid nitrogen. The X-band continuous-wave EPR spectrum was obtained on a Bruker EMX spectrometer at 77K in a liquid nitrogen dewar using Bruker Win-EPR software (ver. 3.0). Data were collected at under non-saturating conditions with the following acquisition parameters: microwave frequency = 9.347 GHz; temperature = 77K; microwave power = 2.07e-3 mW; modulation amplitude = 1 Gauss; conversion time = 40.96 ms.

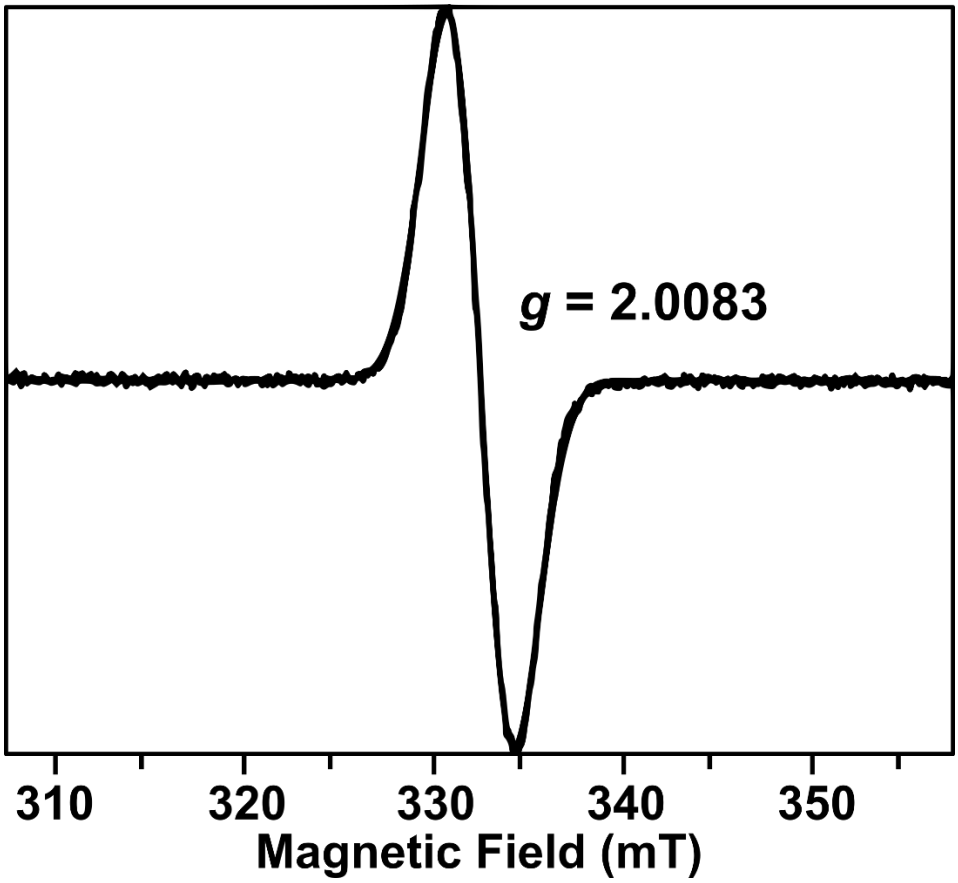

Figure S14. X-band continuous wave EPR spectrum of [**1**][$SbCl_6$] generated *in-situ* from treatment of **1** with [$N(2,4\text{-}Br_2C_6H_3)_3$][$SbCl_6$] (toluene).

S6. One-electron reduction of [1][SbCl$_6$] to 1 with ferrocene

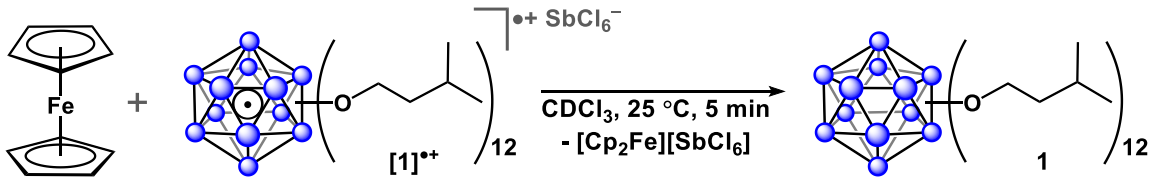

The [**1**][SbCl$_6$] (0.013 mmol) salt was freshly prepared according to the procedure described in **Section S2.3**. The dark yellow brown solids were dissolved in $CDCl_3$ (0.5 mL) and transferred to an NMR tube. The tube was brought outside of the glovebox and ^{1}H (**Figure S15**, top) and ^{11}B{^{1}H} NMR spectra (**Figure S16**, top) were immediately collected to confirm the clean formation of [**1**][SbCl$_6$]. The NMR sample was then transferred back into the glovebox, and to this solution was added a $CDCl_3$ solution (0.4 mL) of ferrocene (5 mg, 0.03 mmol, 2 equiv), which resulted in the immediate formation of dark blue-green precipitate. The reaction mixture was filtered through a piece of microfiber glass filter paper and the yellow-orange filtrate was transferred to an NMR tube. The ^{1}H (**Figure S15**, bottom) and ^{11}B{^{1}H} NMR spectra (**Figure S16**, bottom) that were immediately collected display resonances consistent with the *hypercloso*-**1** cluster.

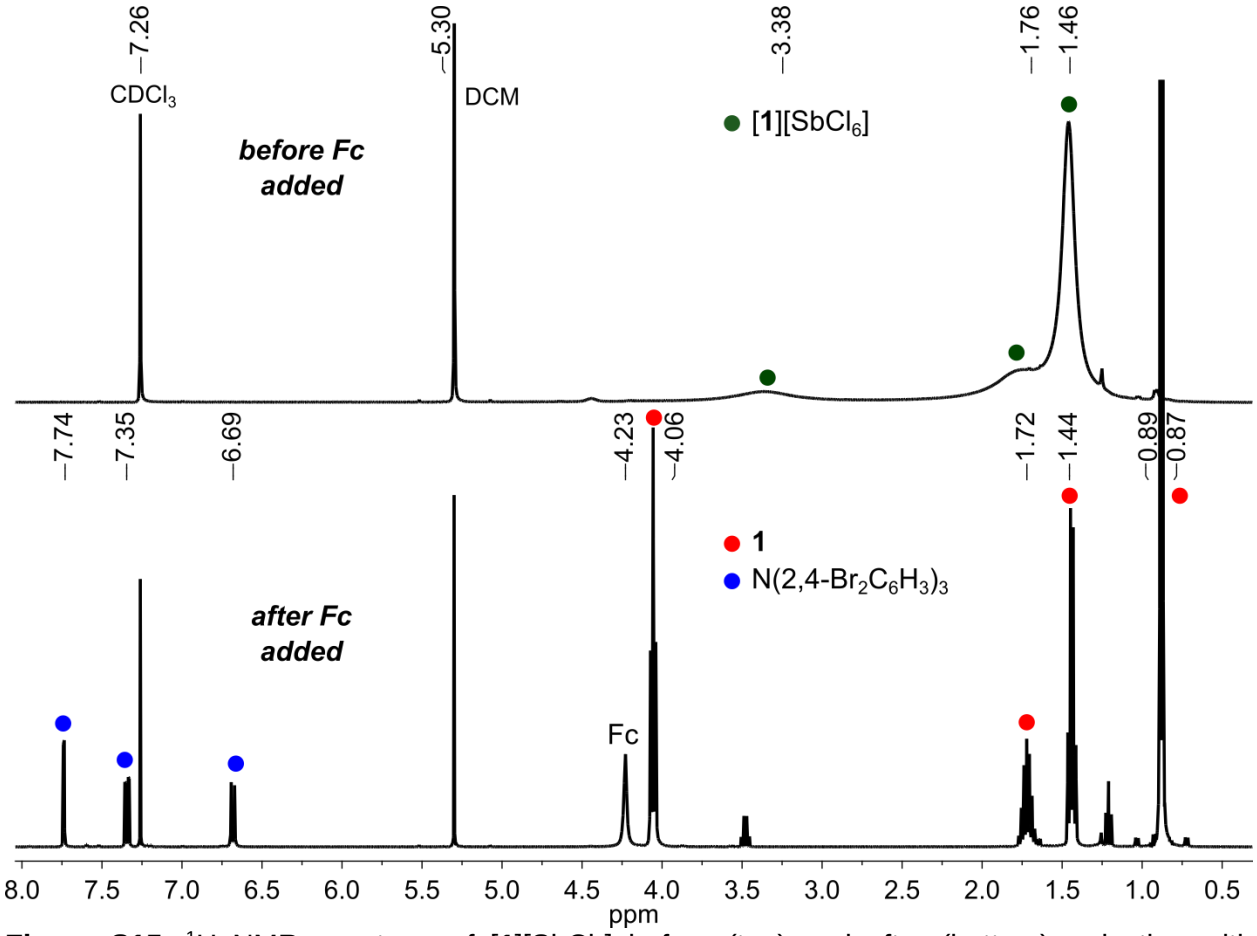

Figure S15. ^{1}H NMR spectrum of [**1**][SbCl$_6$] before (top) and after (bottom) reduction with ferrocene. The spectrum after the reduction of [**1**][SbCl$_6$] with ferrocene displays ^{1}H NMR resonances attributed to *hypercloso*-**1** (•) ($CDCl_3$, 400 MHz, 25 °C).

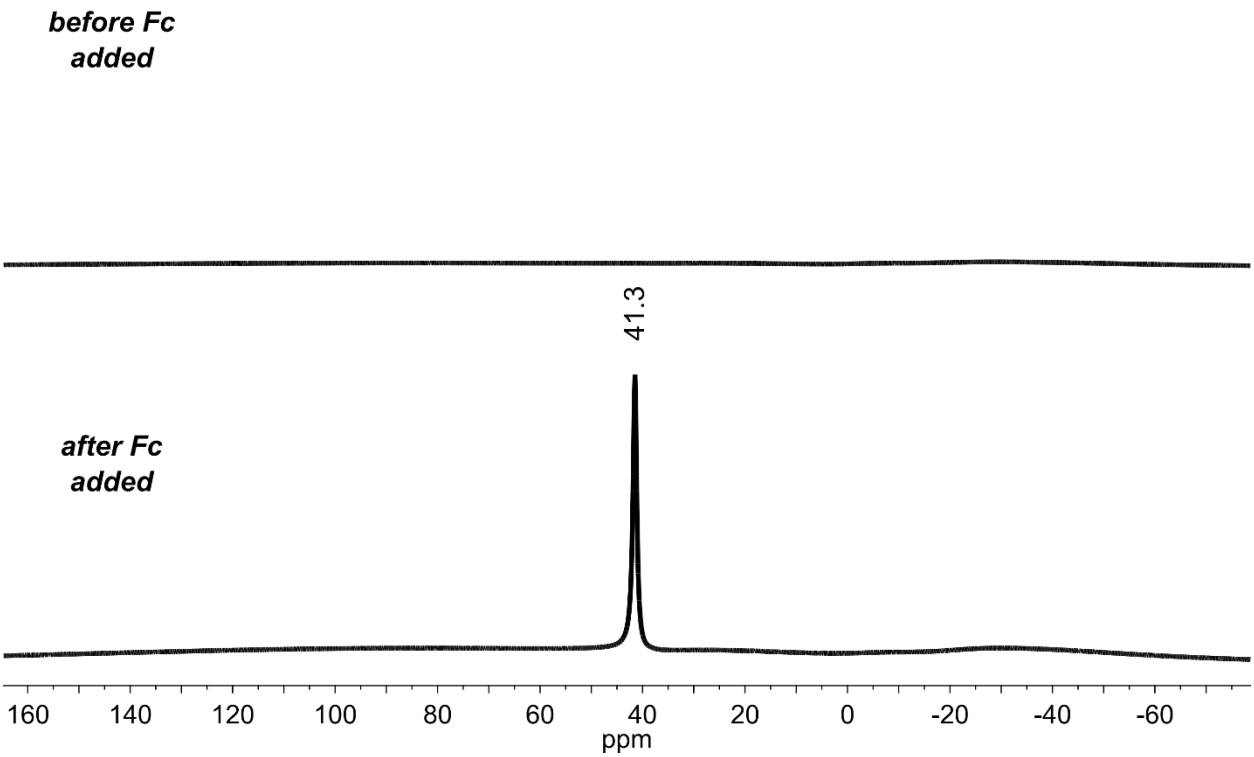

Figure S16. $^{11}B\{^{1}H\}$ NMR spectrum of [**1**][$SbCl_6$] before (top) and after (bottom) reduction with ferrocene. The spectrum after the reduction of [**1**][$SbCl_6$] with ferrocene displays the ^{11}B NMR resonance attributed to *hypercloso*-**1** (δ 41.3 ppm) ($CDCl_3$, 128 MHz, 25 °C).

S7. NMR stability study of [1][SbCl$_6$]

A dark yellow-brown C_6D_6 (0.6 mL) solution of freshly prepared [**1**][$SbCl_6$] (10 mg, 0.0066 mmol) was transferred to an NMR tube, and ^1H and $^{11}B\{^1H\}$ NMR spectra were collected immediately. The solution was allowed to stand undisturbed at 25 °C for 2 h and then ^1H and $^{11}B\{^1H\}$ NMR spectra were collected again. ^1H and $^{11}B\{^1H\}$ NMR spectra were subsequently collected after the solution was allowed to stand for a total of 4 h, at which point full conversion of [**1**][$SbCl_6$] back to **1** was judged by the absence of ^1H NMR resonances corresponding to [**1**][$SbCl_6$] and the presence of ^1H and ^{11}B NMR resonances attributed to **1**. Other new resonances assigned to cluster-based reduced diamagnetic decomposition products that have yet to be identified were observed in the ^1H and $^{11}B\{^1H\}$ NMR spectra collected after 4 h. Investigation into the oxidized organic byproduct(s) generated during the reduction of [**1**]$^{\bullet+}$ to **1** are also underway.

This study displays the extremely high reactivity of the [**1**]$^{\bullet+}$ species in solution, which contributed to the difficulty we had in growing X-ray quality crystals of the intact, oxidized [**1**]$^{\bullet+}$ cluster for structural characterization.

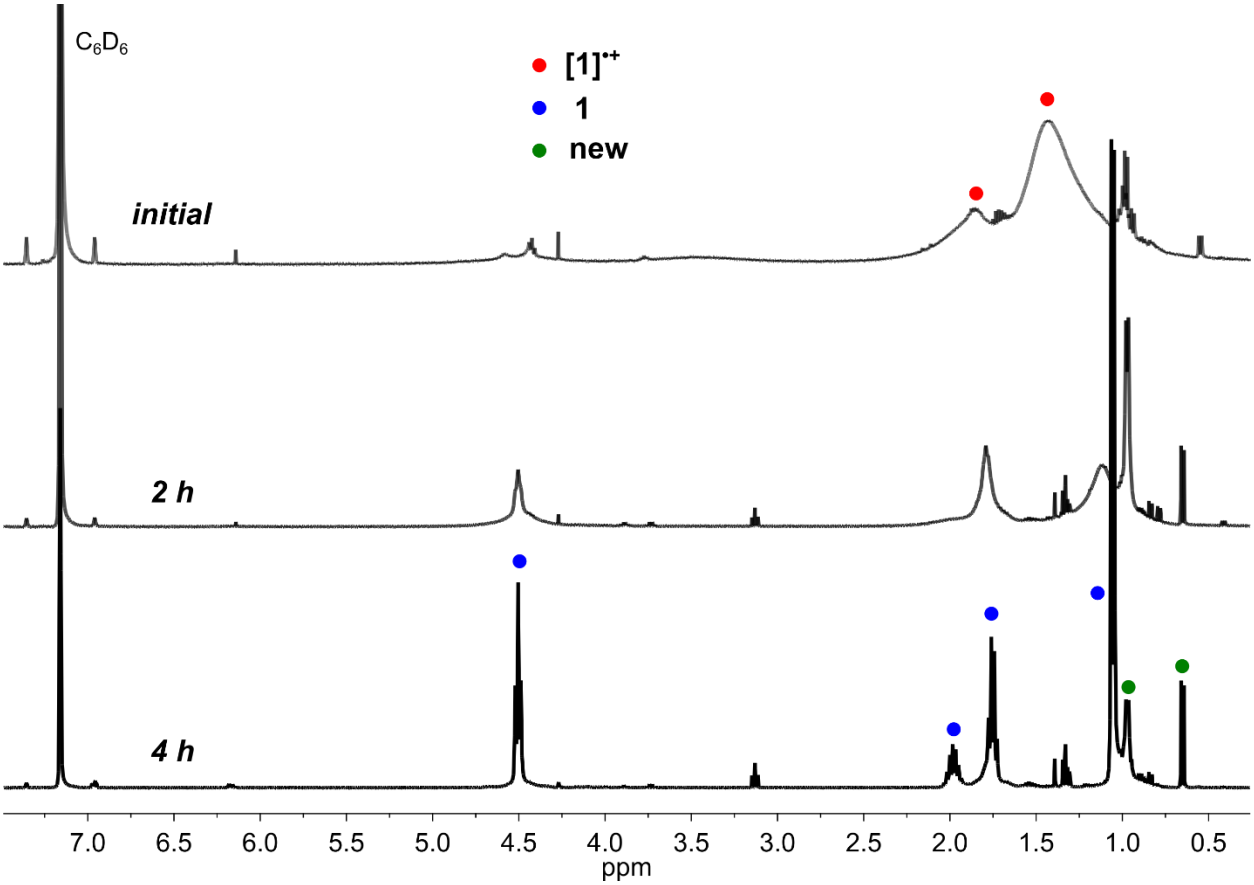

Figure S17. ^1H NMR spectra of [**1**][$SbCl_6$] collected immediately (top), after standing for 2 h at 25 °C (middle), and after standing for 4 h at 25 °C in C_6D_6 (bottom). After standing for 4 h in C_6D_6, full conversion of [**1**][$SbCl_6$] (•) to **1** (•) is observed in addition to the formation of diamagnetic cluster-based decomposition products (•) (C_6D_6, 400 MHz, 25 °C).

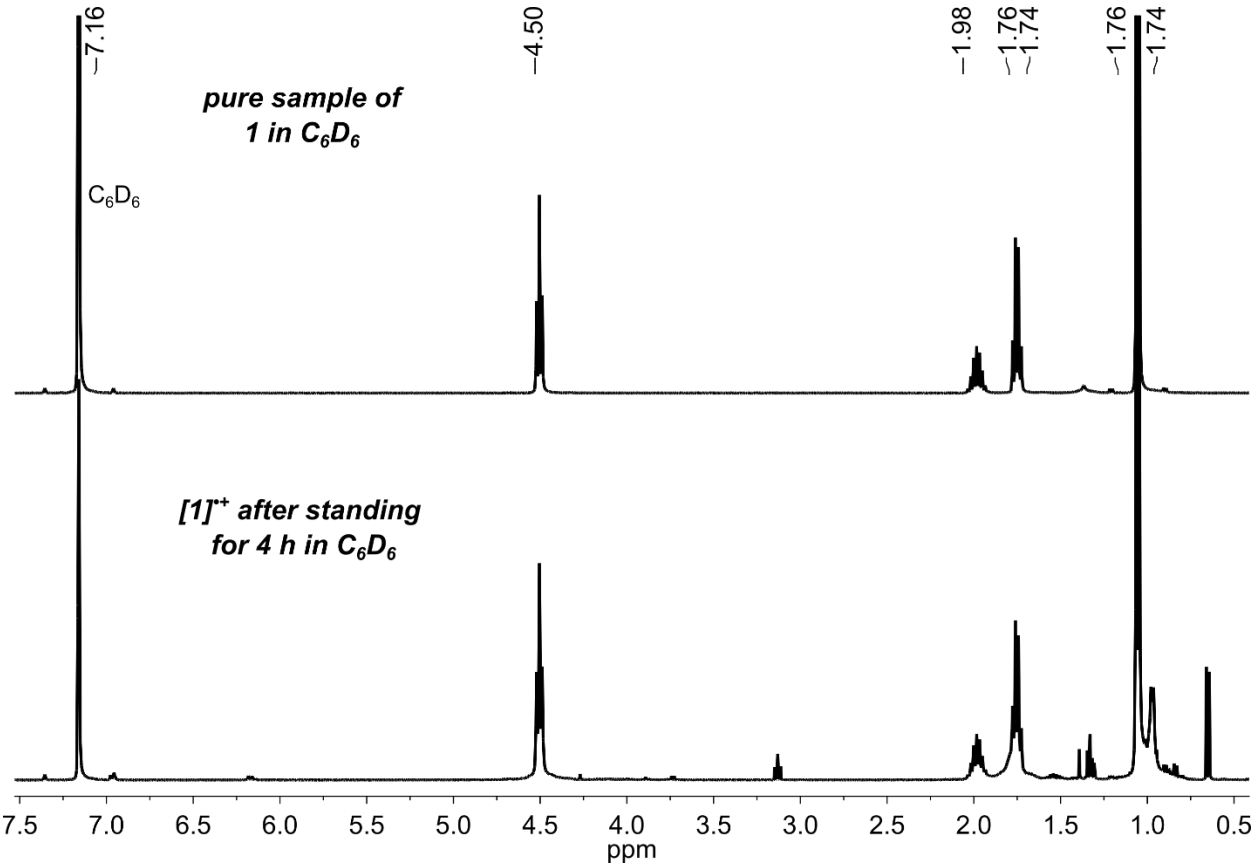

Figure S18. ^{1}H NMR spectrum of a pure sample of **1** in C_6D_6 (top), and spectrum of [**1**][$SbCl_6$] after standing for 4 h at 25 °C in C_6D_6 (bottom) showing resonances consistent with **1** (C_6D_6, 400 MHz, 25 °C).

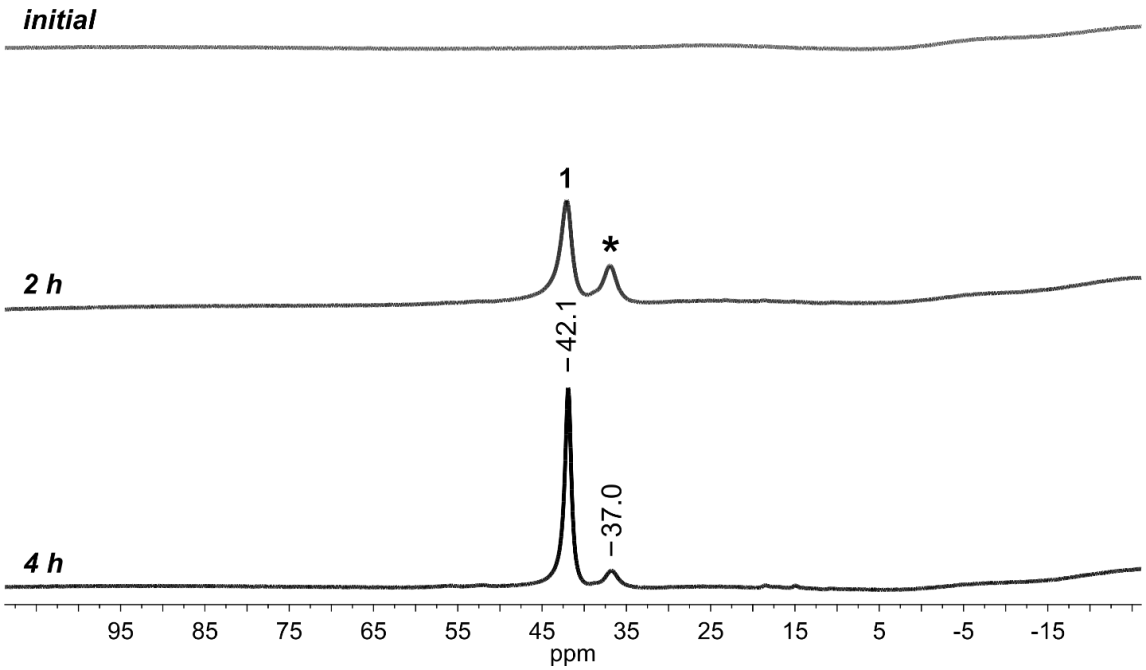

Figure S19. $^{11}B\{^{1}H\}$ NMR spectra of [**1**][$SbCl_6$] collected immediately (top), after standing for 2 h at 25 °C (middle), and after standing for 4 h at 25 °C in C_6D_6 (bottom). After standing for 4 h in C_6D_6, full conversion of [**1**][$SbCl_6$] to **1** (δ 42.1 ppm) was observed in addition to the formation of a diamagnetic decomposition product (resonance indicated with *****) (C_6D_6, 128 MHz, 25 °C).

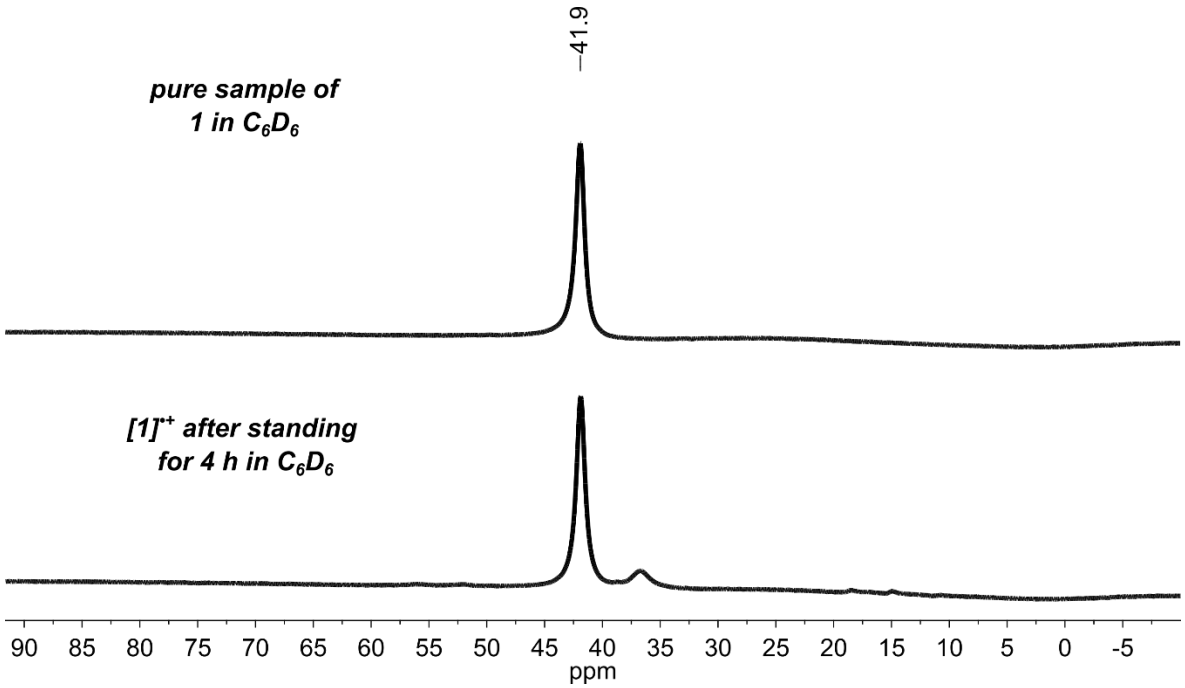

Figure S20. $^{11}B\{^{1}H\}$ NMR spectrum of a pure sample of **1** in C_6D_6 (top), and spectrum of [**1**][$SbCl_6$] after standing for 4 h at 25 °C in C_6D_6 (bottom) showing a resonance consistent with **1** (C_6D_6, 128 MHz, 25 °C).

S8. Attempted preparation of $[1]^{\bullet-}$: treatment of 1 with hydrazine

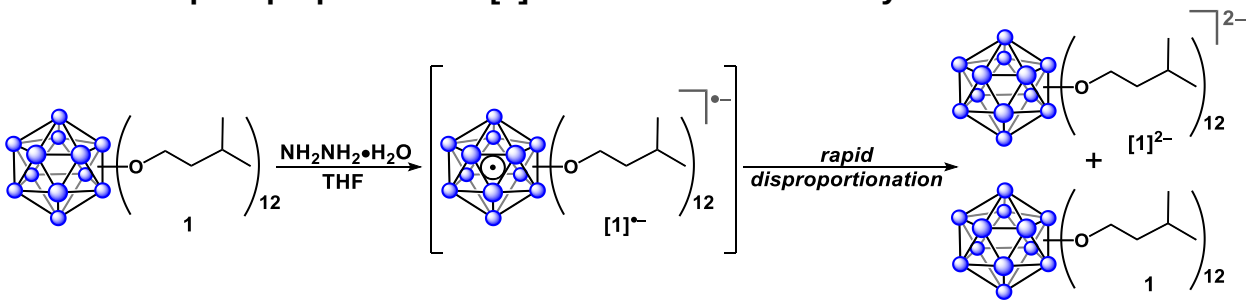

In the fume hood open to air, N_2H_4•H_2O (1 µL, 0.01 mmol, 2 equiv) was added to a dark yellow solution of **1** (10 mg, 0.0066 mmol, 1.0 equiv) in THF-d_8 (0.5 mL) at ambient temperature. The color of the reaction mixture became bright pink immediately upon addition. The pink solution was then transferred to an NMR tube and ^{1}H (**Figure S21**) and ^{11}B{^{1}H} NMR (**Figure S23**) spectra were collected immediately. Both ^{1}H and ^{11}B{^{1}H} NMR spectra display diamagnetic resonances corresponding to **1** and $[\mathbf{1}]^{2-}$. Based on its redox potential ($E_{1/2}$ -0.4 V),[5] N_2H_4 is not a strong enough reducing agent to effect the two-electron reduction of **1** to $[\mathbf{1}]^{2-}$ ($E_{1/2}$ $[\mathbf{1}]^{\bullet-/2-}$ = -1.291 V). The fact that the **1** and $[\mathbf{1}]^{2-}$ species are present after treatment of **1** with N_2H_4 suggests that initial formation of $[\mathbf{1}]^{\bullet-}$ is followed by its rapid disproportionation to **1** and $[\mathbf{1}]^{2-}$.

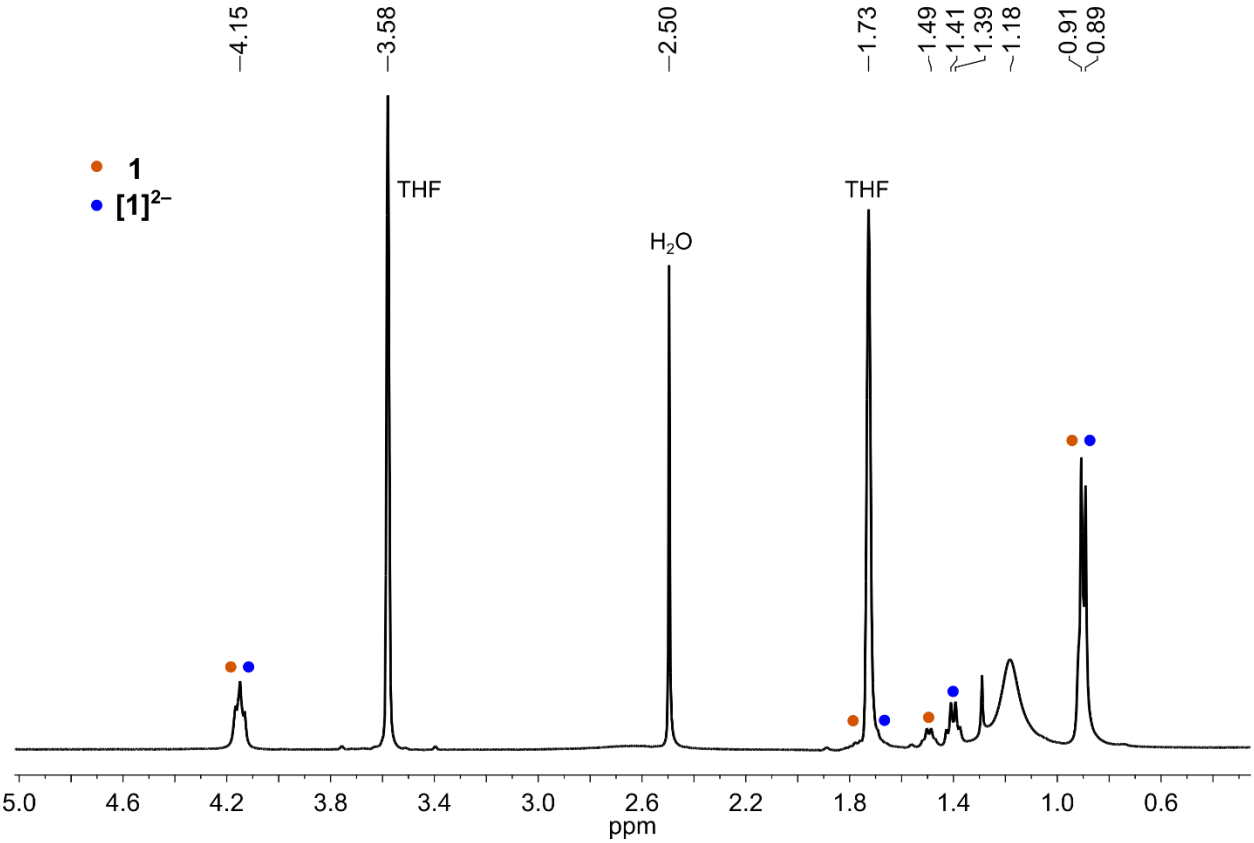

Figure S21. ^{1}H NMR spectrum of the crude reaction mixture displaying the presence of **1** (•) and $[\mathbf{1}]^{2-}$ (•) (THF-d_8, 400 MHz, 25 °C).

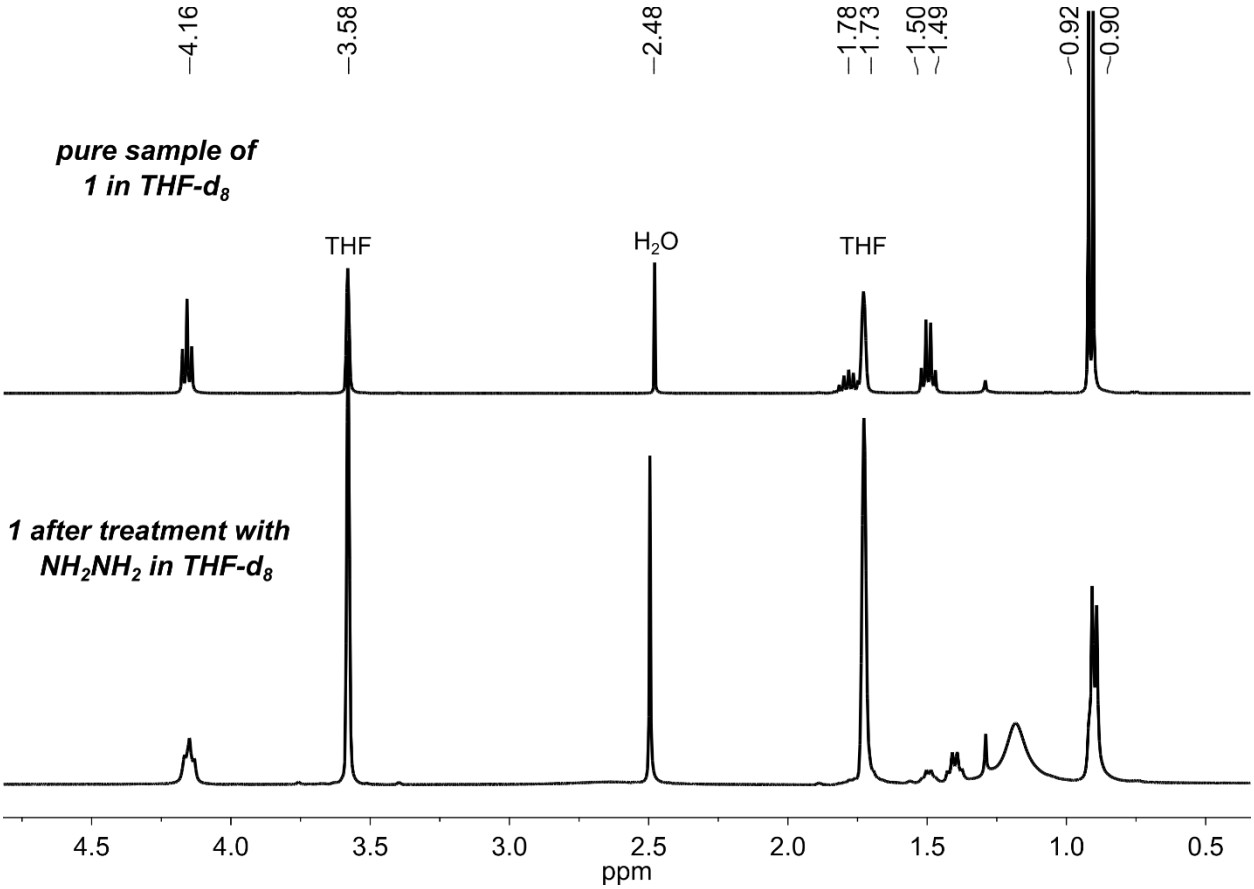

Figure S22. ^{1}H NMR spectrum of a pure sample of **1** in THF-d_8 (top), and spectrum after treatment of **1** with NH_2NH_2 in THF-d_8 (THF-d_8, 400 MHz, 25 °C).

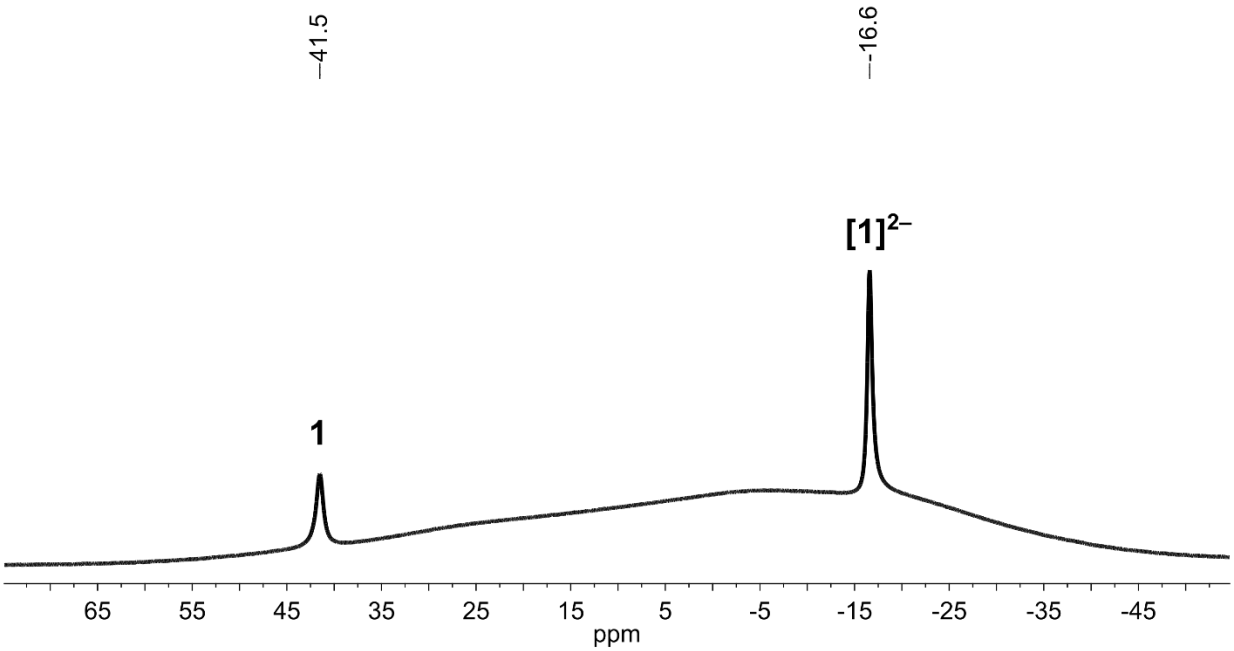

Figure S23. $^{11}B\{^{1}H\}$ NMR spectrum of the crude reaction mixture displaying the presence of **1** (δ -41.5 ppm) and $[\mathbf{1}]^{2-}$ (δ -16.6 ppm) (THF-d_8, 128 MHz, 25 °C).

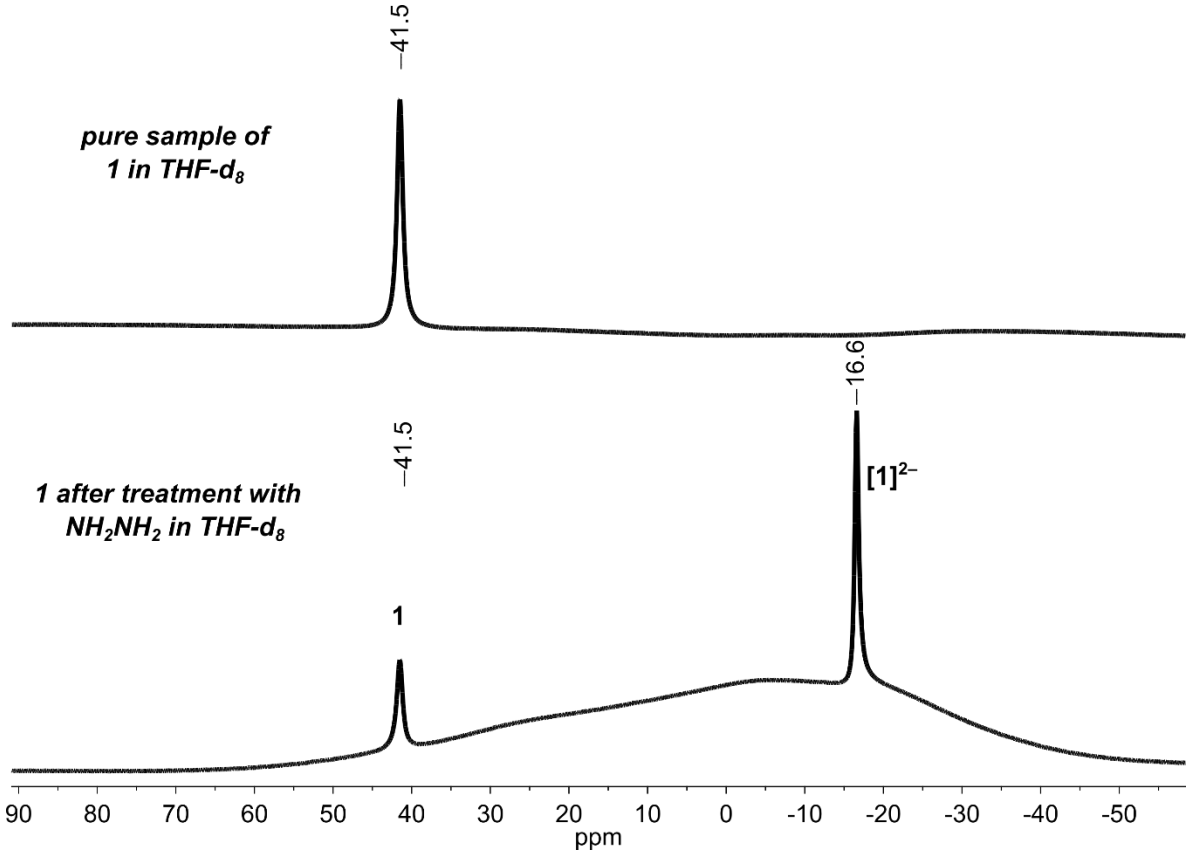

Figure S24. $^{11}B\{^{1}H\}$ NMR spectrum of a pure sample of **1** in THF-d_8 (top), and spectrum after treatment of **1** with NH_2NH_2 in THF-d_8 (THF-d_8, 128 MHz, 25 °C).

S9. Computational details

S9.1. Methods

Density functional theory (DFT) calculations were performed with *Gaussian 16* rev. C.01.[6] To find the best functional for the system, geometry optimizations were carried out separately using B3LYP,[7–10] B3LYP with Grimme's dispersion with Becke-Johnson damping[11] (Gaussian keyword "empiricaldispersion=GD3BJ"), denoted herein B3LYP-D3 and CAM-B3LYP[12] functionals with a Pople split-valence double-ζ basis set[13] 6-31G(d) for all atoms. Geometry minima on the potential energy surface (PES) were confirmed as such by harmonic frequency analysis, showing zero imaginary frequency, at the same level of theory. Gibbs energies were evaluated at 298.15K, using a quasi-rigid rotor harmonic oscillator (quasi-RRHO) treatment of vibrational entropies[14,15] at a cut-off of 100 cm^{-1}. Briefly, a free-rotor approximation was used for all vibrational frequencies less than 100 $cm^{-1}$and a damping function was used to interpolates between the RRHO and the free-rotor vibrational entropy to avoid a discontinuity. The values were further corrected at 1 mol L^{-1} when going from gas-phase to the solution phase.

For time-dependent DFT (TD-DFT) calculations, CAM-B3LYP functional was adopted due to its robust performance for the study of excited states.[16,17] In this case, 6-31+G(d,p) basis set[13] for all atoms was used. The SMD continuum solvation model[18] was used to account for the implicit solvent effect of dichloromethane (DCM), which was the solvent used for UV-vis measurements. For UV-vis spectra, Gaussian function, with a standard deviation of wavenumber (σ) of 0.4 eV, was used to broaden the peaks, as described on the *Gaussian 16* webpage.[19]

For electrochemical potential estimation, the solvation energies were calculated at at B3LYP-D3/def2-SVP[20–22] level of theory using SMD model for DCM, at geometries optimized at B3LYP-D3/6-31G(d) level of theory (we denote this model chemistry as SMD(DCM)-B3LYP-D3/def2-SVP//B3LYP-D3/6-31G(d)). For ^{11}B NMR calculations, using the B3LYP-D3 optimized geometries, the chemical shielding tensors were calculated at B3LYP/def2-SVP level of theory with SMD solvation model to account for the effect of chloroform solvent. The Gauge-Including Atomic Orbitals (GIAOs)[23] method with the Gaussian keyword "nmr = (GIAO,Mixed)" was used. This level of theory (B3LYP/def2-SVP) has been shown to be computationally efficient and to give good agreement with experimental measurements for a variety of boron-containing compounds.[24,25]

Molecular orbitals were visualized using an isosurface value of 0.05 a.u. throughout. All molecular structures and molecular orbitals were visualized using *PyMOL* software.[26] Coordinates of the optimized geometries have been deposited within this Supporting Information (**Section S9.8**).

S9.2. Geometry optimization and structural comparison of 1 and [1]$^{\bullet+}$

Geometry optimizations were carried out on the **1** and [**1**]$^{\bullet+}$ clusters at the B3LYP[7,9,10,27]-D3BJ/6[28]-31G(d)[13] level of theory and the optimized structures are given in **Figure S25**. These calculations show that the geometry of **1** is not significantly altered upon single-electron oxidation as indicated by the small RMSD when the two structures are aligned (RMSD = 0.196 Å). The B–O bond lengths of [**1**]$^{\bullet+}$ are shortened on average by ca. 0.02 Å when compared with those of **1**, suggesting that the B–O bonds are strengthened upon cluster oxidation. The B–B bond lengths show greater variability, suggesting some degree of geometrical distortion upon oxidation. This deviation from idealized icosahedral symmetry is consistent with Jahn-Teller distortion observed crystallographically for the oxidized, D_{3d} symmetric *hypercloso* species when compared with their reduced *hypocloso* and *closo* I_h symmetric analogues.[1,3,29]

1	**[1]$^{\bullet+}$**
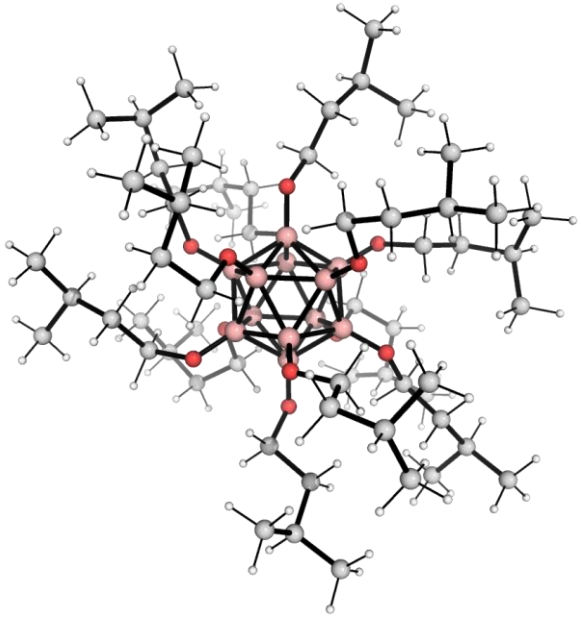	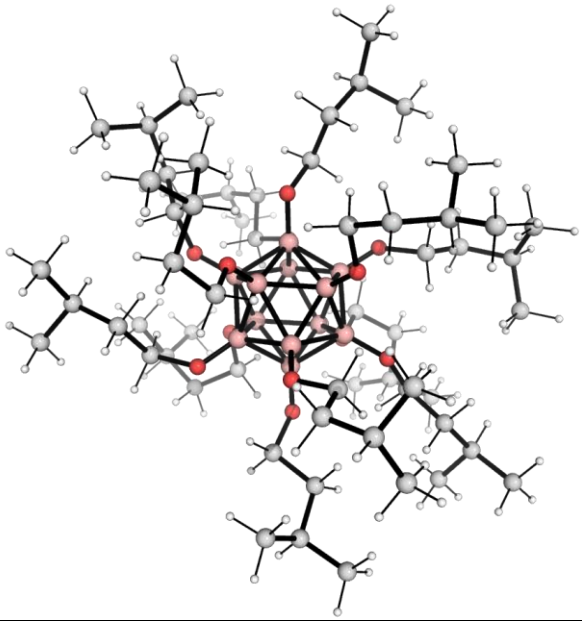
Alignment (RMSD = 0.196 Å)	
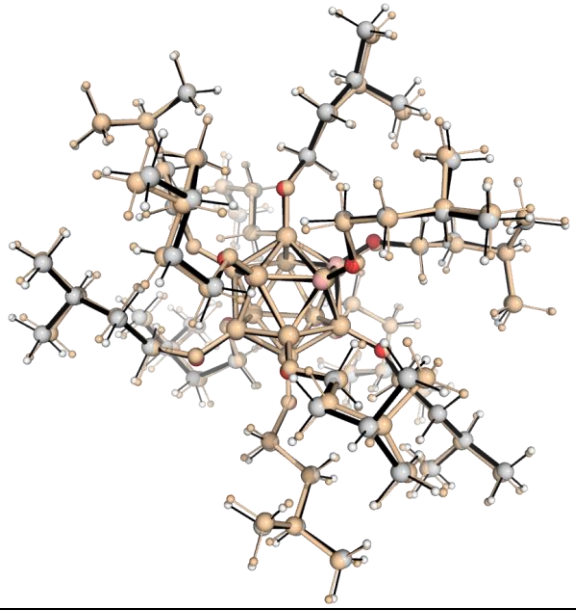	

Bond length (Å)		
Bond	**1**	**$[1]^{\bullet+}$**
B–B (type 1)	1.73	1.75; 1.76
B–B (type 2)	1.84; 1.85	1.80; 1.81; 1.82; 1.86; 1.87; 1.89
B–O	1.39	1.37

Figure S25. B3LYP-D3 optimized geometry of **1** and $[\mathbf{1}]^{\bullet+}$ and key bond lengths in Å. Their structural alignment is given, with $[\mathbf{1}]^{\bullet+}$ displayed in black/gray superimposed on **1**, which is displayed in pale pink. The naming of B–B bond lengths as "type 1" vs "type 2" is arbitrary.

S9.3. Calculated UV-vis spectra of 1 and $[1]^{\bullet+}$

For all UV-vis spectra calculations, we used TD-DFT SMD(DCM)-CAM-B3LYP/6-31+G(d,p)//B3LYP-D3/6-31G(d) with 50 excited states for simulation.

S9.3.1. 1

The main transitions giving rise to the peaks shown in **Figure *S26*** are given in **Table S1**. All transitions arise from exciting the electrons from the lower occupied orbitals to the LUMO of the molecule (MO # 325). The peak at ~450 nm arises from the transitions from HOMO-5 (MO # 319), HOMO-4 (MO # 320) and HOMO-3 (MO # 321) to the LUMO, as shown in **Table S1**. The selected MOs are given in **Figure S27**. The electron distributions are centered around the B_{12} cluster and the O-atoms of the cluster and are rarely on the alkyl side chains.

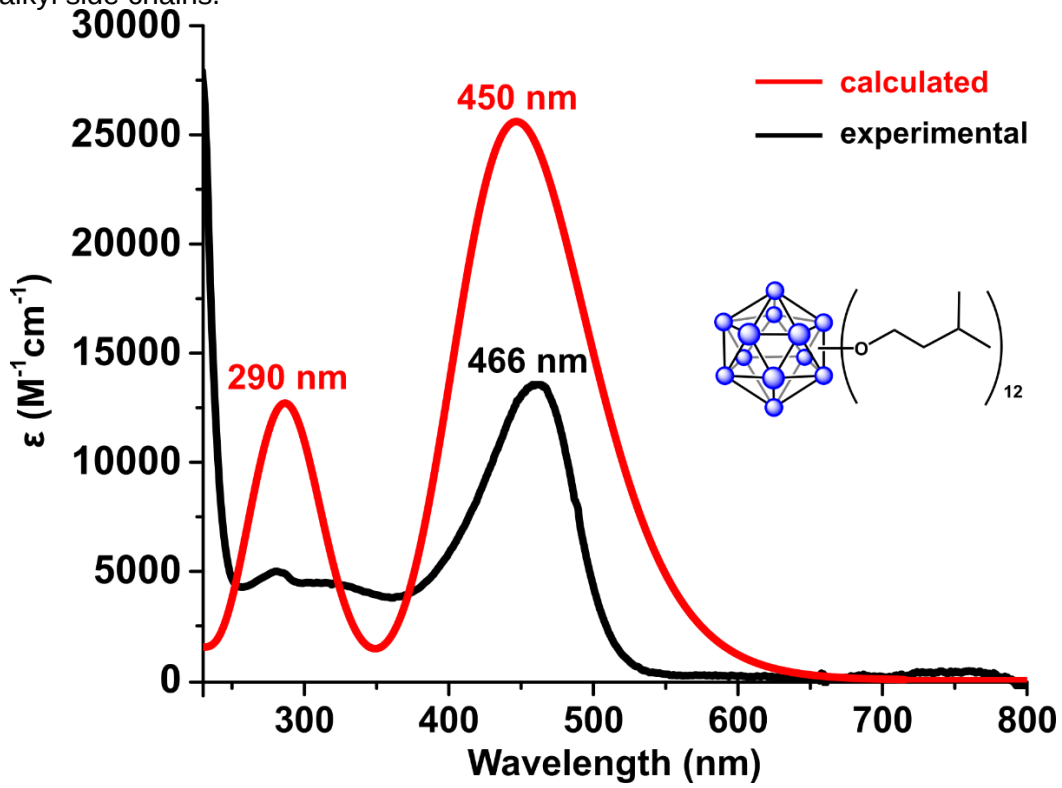

Figure S26. Calculated and experimental (DCM, 80 µM) UV-vis spectra of **1**.

Excited State No.	Excitation Energy / eV	Absorption Wavelength / nm	Oscillator Strength	MO transitions	Contribution
4	2.7313	453.95	0.2002	321 → 325	0.975
5	2.7598	449.24	0.2309	320 → 325	0.974
6	2.8363	437.14	0.2087	319 → 325	0.974
8	4.028	307.8	0.0142	272 → 325 311 → 325 312 → 325 313 → 325 314 → 325 316 → 325 318 → 325	0.043 0.042 0.096 0.043 0.272 0.031 0.336
9	4.155	298.4	0.059	311 → 325 314 → 325 316 → 325 317 → 325 318 → 325	0.022 0.090 0.094 0.380 0.308
11	4.2043	294.9	0.0735	312 → 325 314 → 325 315 → 325 316 → 325 317 → 325	0.027 0.023 0.357 0.476 0.043
12	4.2816	289.58	0.0536	308 → 325 311 → 325 312 → 325 314 → 325 315 → 325 316 → 325 317 → 325	0.031 0.044 0.408 0.274 0.053 0.033 0.036
13	4.3216	286.89	0.0298	310 → 325 312 → 325 313 → 325 314 → 325 315 → 325	0.035 0.029 0.725 0.061 0.020
15	4.4551	278.3	0.034	302 → 325 309 → 325 310 → 325 311 → 325 313 → 325	0.047 0.097 0.543 0.041 0.051
16	4.5389	273.16	0.0128	303 → 325 304 → 325 306 → 325 307 → 325 308 → 325 311 → 325 312 → 325	0.046 0.044 0.424 0.103 0.087 0.032 0.022
18	4.6087	269.02	0.0332	277 → 325 285 → 325 304 → 325	0.039 0.032 0.104

				305 → 325 306 → 325 307 → 325 309 → 325 310 → 325 311 → 325	0.024 0.081 0.399 0.047 0.060 0.022
19	4.6673	265.65	0.031	270 → 325 271 → 325 298 → 325 303 → 325 304 → 325 305 → 325 306 → 325 307 → 325 308 → 325 309 → 325 311 → 325	0.026 0.029 0.043 0.050 0.033 0.040 0.081 0.021 0.270 0.158 0.053
20	4.7035	263.6	0.0198	268 → 325 298 → 325 300 → 325 302 → 325 303 → 325 304 → 325 305 → 325 306 → 325 307 → 325 308 → 325 309 → 325	0.022 0.042 0.036 0.023 0.026 0.106 0.182 0.022 0.046 0.224 0.022

Table S1. Computed electronic transitions for **1**. Oscillator strengths greater than 0.01 are included. For **1**, MO #325 is the HOMO and MO #324 is the LUMO.

LUMO (MO #325)	HOMO (MO #324)
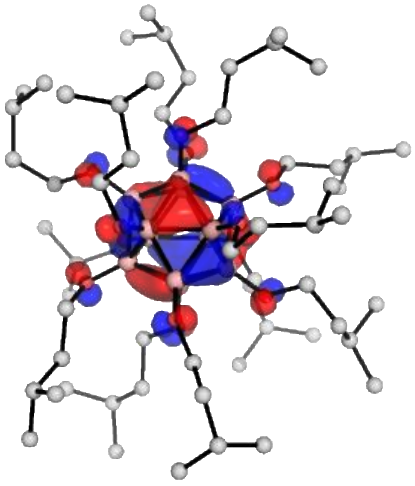	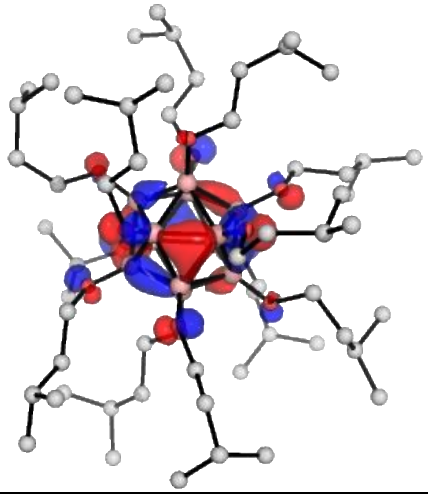
HOMO-3 (MO #321)	**HOMO-4 (MO #320)**
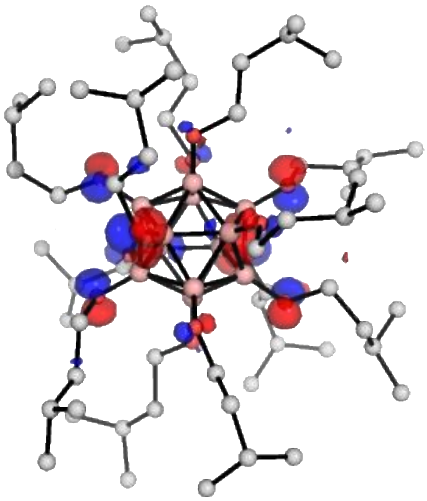	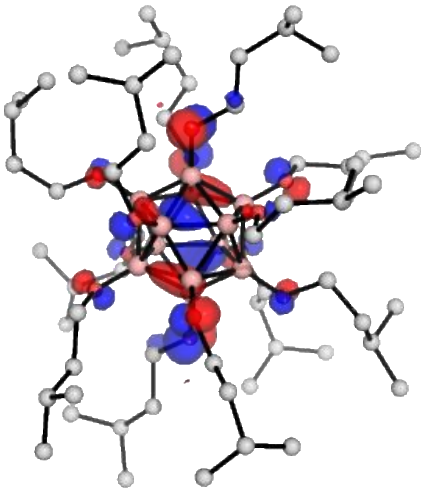
HOMO-5 (MO #319)	
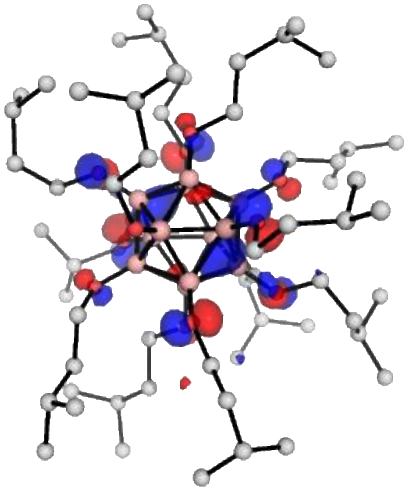	

Figure S27. Selected MOs for **1**. H-atoms are hidden for clarity.

S9.3.2. $[1]^{\bullet+}$

The peaks arise from transitions from the lower occupied MOs to the LUMO (MO #325A) of the α-spin orbitals and the LUMO (MO #324B) and LUMO+1 (MO #325B) of the β-spin orbitals (**Table S2**). The computed transition around 820 nm, which likely corresponds to the experimentally observed peak at 720 nm, arises from the excitations from the ground state to excited states 7, 9 and 10, which result from the excitation of β-electron from MOs #319B, 320B, 321B to β-spin LUMO #324B (**Table S2**). These MOs are shown in **Figure S29**. These suggest that the long-wavelength transition in the $[\mathbf{1}]^{\bullet+}$ system (inset, **Figure S28**) arise from charge transfer from the periphery (O-atoms) to the B_{12}-core. The peak at around 464 nm arises from the transition from the ground state to the excited states 14, 15 and 16, where both α- and β-electronic transitions occur (the dominant contributions are given in bold in **Table S2**).

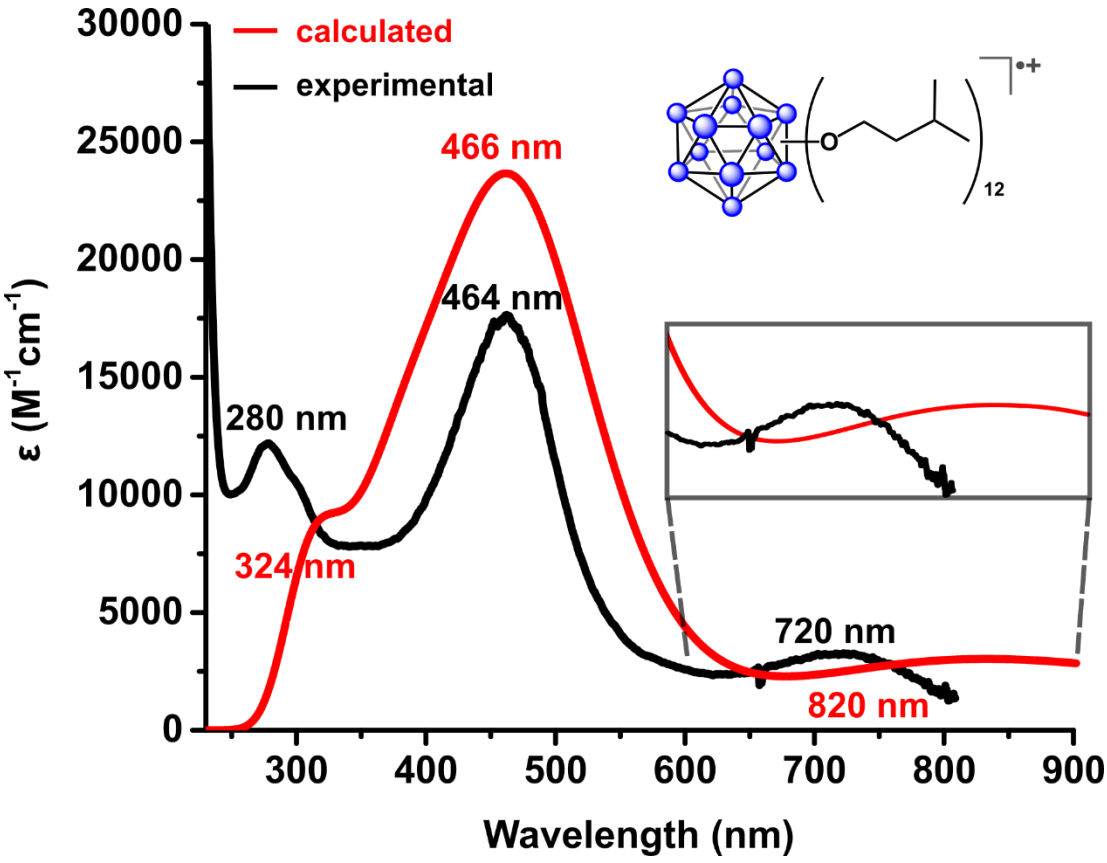

Figure S28. Calculated and experimental (DCM, 70 µM) UV-vis spectra of $[\mathbf{1}]^{\bullet+}$.

Excited State No.	Excitation Energy / eV	Absorption Wavelength / nm	Oscillator Strength	MO transitions	Contribution
7	1.3921	890.65	0.0337	319A → 325A 321A → 325A 323A → 325A 320B → 325B **321B → 324B** 323B → 325B	0.013 0.066 0.017 0.022 **0.838** 0.015
9	1.4777	839.03	0.0264	320A → 325A 321A → 325A 319B → 324B **320B → 324B**	0.055 0.020 0.015 **0.864**
10	1.6413	755.39	0.0149	320A → 325A 321A → 325A **319B → 324B** 320B → 324B 321B → 325B	0.027 0.030 **0.765** 0.040 0.091
14	2.5497	486.26	0.171	**320A → 325A** 316B → 324B 320B → 324B 320B → 325B **321B → 325B**	**0.590** 0.010 0.021 0.032 **0.279**
15	2.5782	480.89	0.2123	319A → 325A **321A → 325A** 318B → 324B 319B → 324B **320B → 325B** 321B → 325B	0.011 **0.501** 0.016 0.020 **0.365** 0.018
16	2.7239	455.18	0.1454	**319A → 325A** 321A → 325A 316B → 324B 318B → 324B **319B → 325B** 321B → 324B	**0.459** 0.019 0.012 0.060 **0.348** 0.017
17	3.0231	410.12	0.0802	319A → 325A 276B → 324B 277B → 324B 311B → 324B 312B → 324B 314B → 324B 315B → 324B 317B → 324B 318B → 324B 319B → 325B	0.048 0.019 0.014 0.012 0.027 0.014 0.013 0.229 0.452 0.017
18	3.0785	402.75	0.082	319A → 325A 282B → 324B 307B → 324B 309B → 324B 312B → 324B	0.026 0.022 0.011 0.011 0.011

				313B → 324B 315B → 324B 316B → 324B 317B → 324B 318B → 324B 319B → 325B	0.020 0.017 0.089 0.495 0.137 0.011
20	3.2306	383.78	0.0625	320A → 325A 273B → 324B 274B → 324B 278B → 324B 281B → 324B 300B → 324B 302B → 324B 305B → 324B 309B → 324B 312B → 324B 314B → 324B 315B → 324B 316B → 324B 317B → 324B	0.013 0.017 0.014 0.022 0.015 0.015 0.020 0.010 0.011 0.173 0.017 0.244 0.244 0.039
21	3.2598	380.35	0.0261	276B → 324B 278B → 324B 282B → 324B 307B → 324B 309B → 324B 310B → 324B 311B → 324B 313B → 324B 314B → 324B 315B → 324B 318B → 324B	0.016 0.024 0.022 0.017 0.024 0.044 0.047 0.313 0.219 0.036 0.040
22	3.3367	371.58	0.0262	274B → 324B 279B → 324B 281B → 324B 307B → 324B 310B → 324B 312B → 324B 313B → 324B 314B → 324B 315B → 324B 318B → 325B	0.079 0.026 0.038 0.011 0.025 0.053 0.127 0.383 0.053 0.019
23	3.3628	368.69	0.0283	317A → 325A 273B → 324B 276B → 324B 277B → 324B 297B → 324B 299B → 324B 307B → 324B 308B → 324B 309B → 324B	0.012 0.034 0.020 0.041 0.023 0.022 0.046 0.053 0.014

				311B → 324B 312B → 324B 313B → 324B 315B → 324B 316B → 324B 317B → 324B 318B → 324B	0.096 0.108 0.095 0.022 0.155 0.019 0.010
26	3.5227	351.96	0.015	313A → 325A 316A → 325A 317A → 325A 318A → 325A 270B → 324B 305B → 324B 307B → 324B 308B → 324B 312B → 324B 313B → 324B 313B → 325B 314B → 324B 316B → 325B 318B → 325B	0.024 0.034 0.054 0.061 0.016 0.030 0.045 0.034 0.020 0.013 0.021 0.027 0.076 0.191
33	3.7438	331.17	0.0159	312A → 325A 313A → 325A 314A → 325A 315A → 325A 316A → 325A 318A → 325A 274B → 325B 276B → 325B 299B → 324B 304B → 324B 305B → 325B 307B → 325B 309B → 324B 310B → 324B 310B → 325B 313B → 325B 314B → 324B 314B → 325B 315B → 325B 317B → 325B 318B → 325B	0.014 0.035 0.022 0.024 0.061 0.115 0.015 0.019 0.019 0.015 0.011 0.012 0.020 0.028 0.012 0.063 0.011 0.073 0.022 0.030 0.089
36	3.8123	325.22	0.0108	272A → 325A 273A → 325A 277A → 325A 307A → 325A 308A → 325A 311A → 325A 312A → 325A 313A → 325A 314A → 325A	0.011 0.019 0.015 0.036 0.016 0.117 0.031 0.041 0.016

				316A → 325A 317A → 325A 272B → 324B 301B → 324B 304B → 324B 305B → 324B 306B → 324B 310B → 325B 315B → 325B 316B → 325B 317B → 325B	0.011 0.058 0.027 0.040 0.011 0.012 0.019 0.020 0.028 0.151 0.024
42	3.9195	316.33	0.0107	310A → 325A 311A → 325A 312A → 325A 316A → 325A 317A → 325A 272B → 324B 290B → 324B 295B → 324B 296B → 324B 298B → 324B 299B → 324B 300B → 324B 307B → 325B 309B → 324B 312B → 325B 314B → 325B 317B → 325B 318B → 325B	0.014 0.020 0.026 0.188 0.026 0.045 0.020 0.033 0.040 0.038 0.012 0.015 0.011 0.010 0.049 0.013 0.059 0.026
44	3.9597	313.12	0.0323	307A → 325A 312A → 325A 313A → 325A 315A → 325A 316A → 325A 318A → 325A 270B → 324B 273B → 324B 274B → 324B 275B → 324B 299B → 324B 300B → 324B 301B → 324B 302B → 324B 303B → 324B 305B → 324B 308B → 324B 313B → 325B 315B → 325B 316B → 325B 318B → 325B	0.023 0.021 0.021 0.053 0.024 0.024 0.021 0.012 0.011 0.011 0.011 0.011 0.030 0.013 0.040 0.043 0.073 0.067 0.133 0.041 0.027
45	3.9679	312.47	0.0169	278A → 325A	0.012

				279A → 325A	0.017
				307A → 325A	0.032
				309A → 325A	0.011
				312A → 325A	0.010
				313A → 325A	0.070
				314A → 325A	0.068
				315A → 325A	0.054
				316A → 325A	0.037
				317A → 325A	0.050
				318A → 325A	0.028
				293B → 324B	0.011
				299B → 324B	0.029
				303B → 324B	0.012
				305B → 325B	0.010
				307B → 325B	0.041
				309B → 325B	0.013
				312B → 325B	0.012
				313B → 325B	0.013
				314B → 325B	0.030
				315B → 325B	0.042
				316B → 325B	0.056
				317B → 325B	0.062
				318B → 325B	0.011
47	4.0086	309.29	0.0598	308A → 325A	0.019
				312A → 325A	0.019
				313A → 325A	0.026
				314A → 325A	0.088
				315A → 325A	0.027
				318A → 325A	0.057
				275B → 324B	0.015
				293B → 324B	0.011
				301B → 324B	0.015
				305B → 324B	0.118
				307B → 325B	0.019
				308B → 324B	0.010
				313B → 325B	0.121
				314B → 325B	0.055
				315B → 325B	0.033
				318B → 325B	0.039

Table S2. Computed electronic transitions for [**1**]$^{\bullet+}$. Oscillator strengths greater than 0.01 are included. A denotes α-MO; B denotes β-MO, a β-electron is removed from MO #324 of **1**, such that MO #324A is the SOMO of [**1**]$^{\bullet+}$.

MO #325A	MO #324A
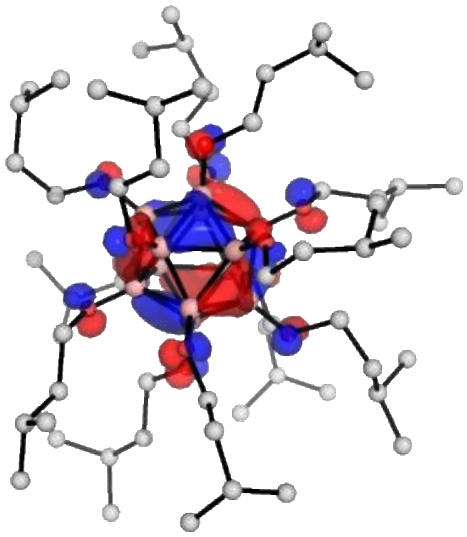	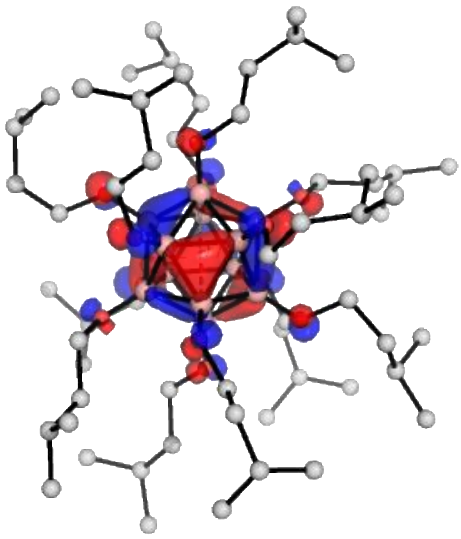
MO #321A	**MO #320A**
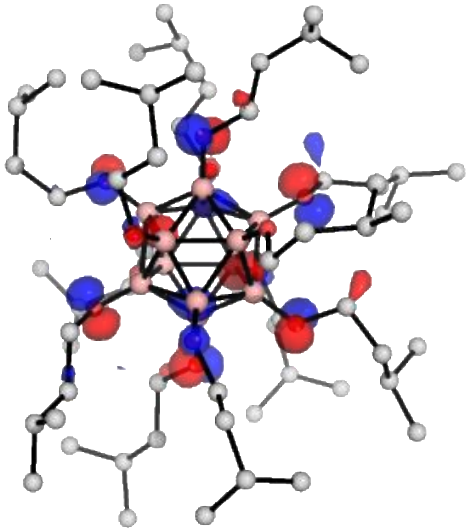	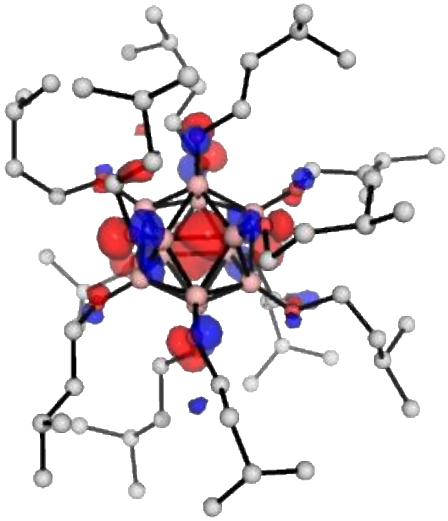
MO #319A	
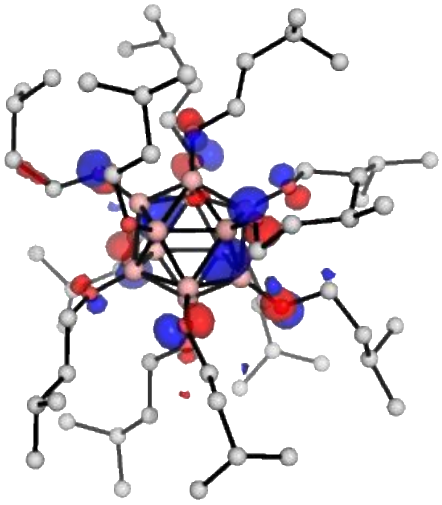	

MO #325B	MO #324B
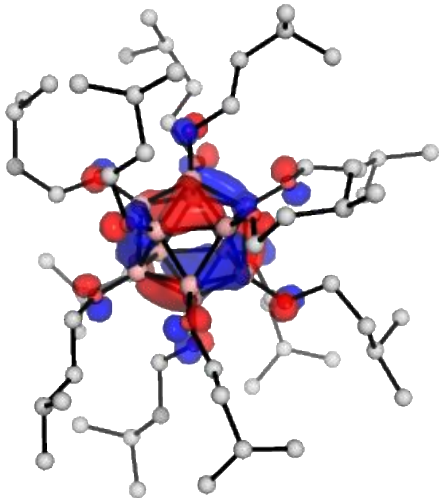	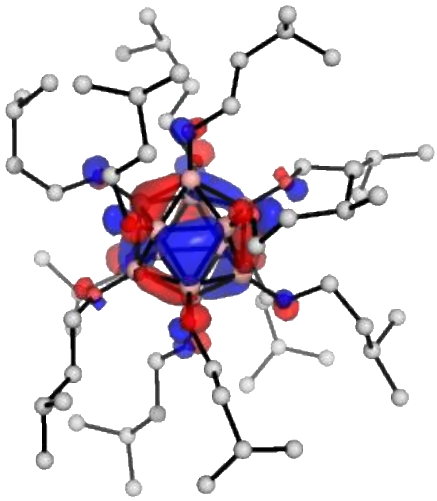
MO #323B	**MO #321B**
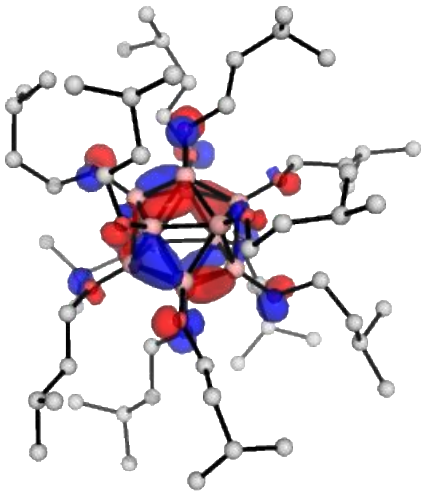	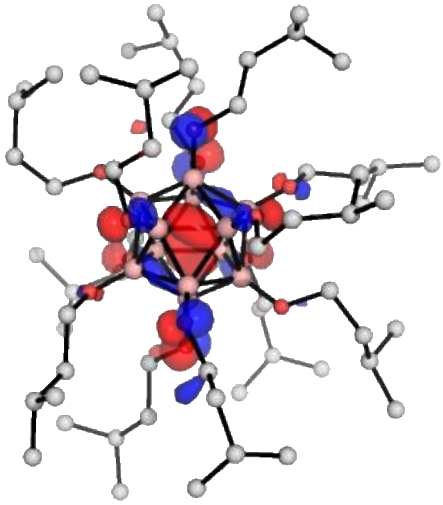
MO #320B	**MO #319B**
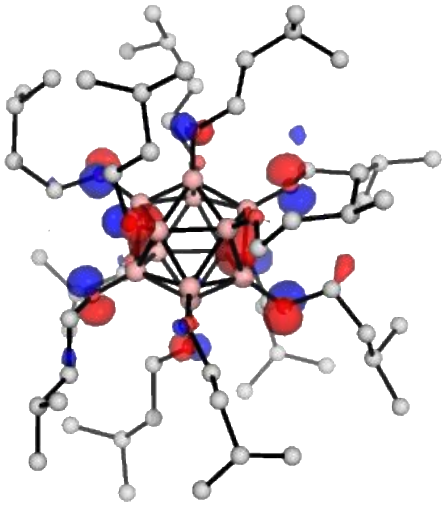	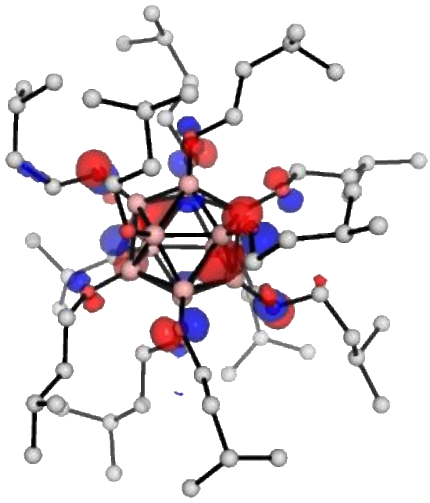

Figure S29. Selected MOs for [**1**]$^{\bullet+}$. H-atoms are hidden for clarity.

S9.4. Electrostatic potential (ESP) of 1 and spin density plot of $[1]^{\bullet+}$

The electrostatic potential (ESP) of **1** and the spin density of the $[\mathbf{1}]^{\bullet+}$ are displayed in **Figure S30**. In *hypercloso*-**1**, the B_{12}-core is positively charged, with the negative charge is localized on the O-atoms. This is perhaps unsurprising given that the oxygen atom is more electronegative than the boron atom. For $[\mathbf{1}]^{\bullet+}$, the unpaired electron/radical is mostly delocalized over the electronegative O atoms and the B_{12}-cluster core, as shown by the spin density plot.

ESP of 1	Spin density plot of $[1]^{\bullet+}$
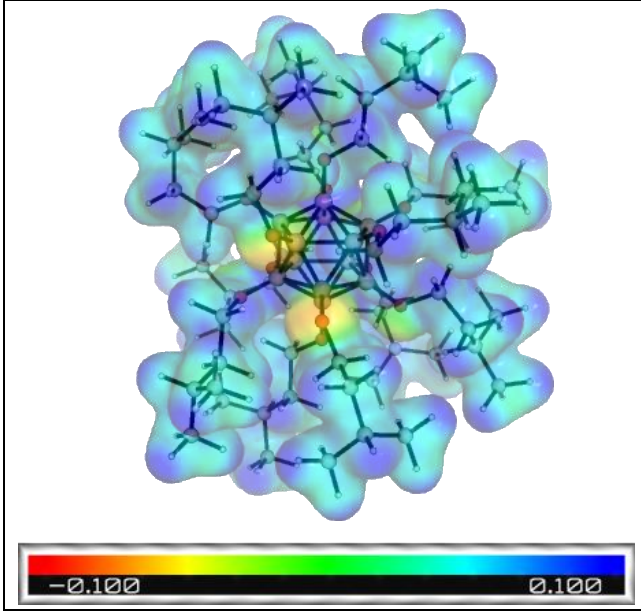	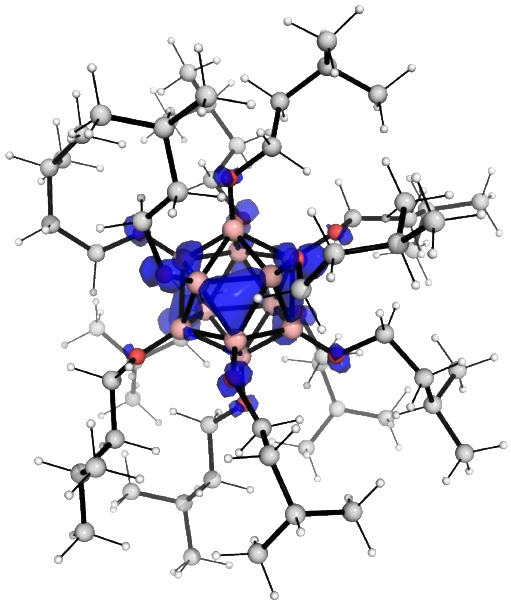

Figure S30. Electrostatic potential (ESP; isovalue of 0.02) of **1** and spin density plot (isovalue of 0.005) of $[\mathbf{1}]^{\bullet+}$.

S9.5. $[1]^{0/\bullet+}$ redox potential calculation

We estimated the adiabatic reduction potential of $[\mathbf{1}]^{\bullet+}$ by constructing a thermodynamic cycle (**Scheme S1**) and using separate gas phase geometry optimizations with single point solvation energy of each *optimized* species (thus the name adiabatic). The overall Gibbs energy of reaction ΔG^o_{rxn} is expressed in terms of the free energy of reaction in the gas phase, ΔG^o_{gas}, and the free energies of solvation, ΔG^o_{solv}, of the reacting species: [30,31]

$$\Delta G^o_{rxn} = -\Delta G^o_{solv}(N^{\bullet+}) - \Delta G^o_{solv}(e^-) + \Delta G^o_{gas}(N^{\bullet+}) + \Delta G^o_{solv}(N)$$

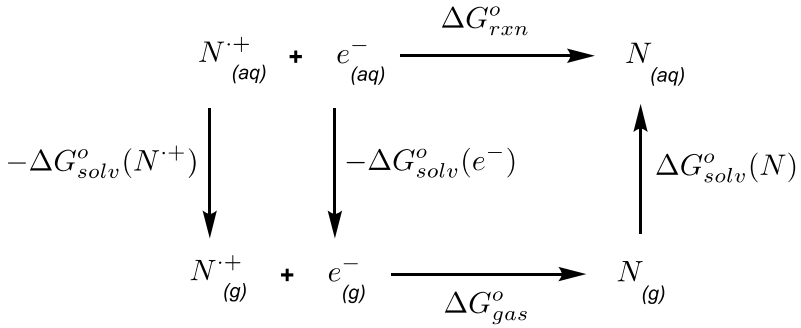

Scheme S1. Computation of the potential for the reduction of $[\mathbf{1}]^{\bullet+}$ to **1**.

The reduction potential of the reaction is then given by:

$$E_{cell} = -\frac{\Delta G^o_{rxn}}{nF} - E_{SHE}$$

where E_{SHE} is the reference potential of the standard hydrogen electrode. We need not consider the free energy of solvation of the electron as their contribution cancels out when we consider the full reaction against experimentally measured values.[31] Using this thermodynamic cycle, we found that the absolute redox potential of the $[\mathbf{1}]^{0/\bullet+}$ couple to be 5.25 V. Together with the absolute redox potential of the ferrocene/ferrocenium (Fc/Fc^+) redox couple of 4.8 ± 0.1 V in dichloromethane,[32] we estimate that the redox potential of the $[\mathbf{1}]^{0/\bullet+}$ couple to be 0.45 ± 0.1 V in dichloromethane (*cf*. experimental value of 0.62 V, **Figure S10**).

S9.6. ^{11}B NMR chemical shift calculation of 1

The ^{11}B NMR chemical shift of **1** was calculated. We adopted SMD(chloroform)-B3LYP/def2-SVP//B3LYP-D3/6-31G(d) level of theory as this gives good agreement with experimental measurements for a variety of boron-containing compounds.[24,25] The computed ^{11}B NMR isotropic shielding tensor value of 113.8 ppm for the reference compound $BF_3{\bullet}OEt_2$ was used as a reference. Averaging the peaks for all boron atoms in **1** gives a final ^{11}B NMR chemical shift of 34.8 ppm (*cf*. experimental value of 41.4 ppm, **Figure S2**). The difference of 6.6 ppm is considered a good agreement due to the wide chemical shift range of >200 ppm for ^{11}B NMR.

S9.7. Absolute energies from the optimized structures

Absolute values (in Hartrees) for SCF energy, zero-point vibrational energy (ZPE), enthalpy and quasi-harmonic Gibbs free energy (at 298K) for optimized structures are given below. Single point (SP) corrections in SMD dichloromethane using B3LYP-D3 functional are also included.

Structure	E/au	ZPE/au	H/au	G/au	qh-G/au	SP
1	-3567.927079	1.950308	-3565.8692	-3566.1275	-3566.0986	-3565.3931
[1]$^{\bullet+}$	-3567.695672	1.9482	-3565.6388	-3565.9023	-3565.8718	-3565.1956

S9.8. Coordinates of the optimized structures

S9.8.1. 1

	x	*y*	*z*
B	0.78966	0.29457	1.56052
O	1.52345	0.73771	2.65876
B	-0.65409	-0.63701	1.77972
O	-1.04347	-1.00634	3.05892
B	0.65572	1.32397	0.03899
O	1.29784	2.55215	-0.07690
C	0.61316	3.79824	0.07167
H	0.03242	3.79455	0.99936
H	-0.10358	3.91446	-0.74786
C	1.64893	4.91151	0.09080
H	2.28828	4.76743	0.97099
H	1.12466	5.86790	0.23271
B	1.58340	-0.13589	-0.04365
O	2.96689	-0.07365	-0.19213
C	3.73462	-1.23397	-0.51703
H	3.66491	-1.41151	-1.59877
H	3.31602	-2.10776	-0.01411
C	5.18000	-0.99000	-0.11465
H	5.48507	-0.01266	-0.50844
H	5.24353	-0.92211	0.98056
B	-0.92645	-1.73942	0.30798
B	-1.04323	1.03255	-0.60624
O	-1.56610	-2.96459	0.43135
O	-1.74857	2.05105	-1.23854
C	-2.00740	2.00801	-2.64610
H	-2.97835	1.52154	-2.80836
H	-1.25094	1.39955	-3.14134
C	-2.02117	3.42848	-3.19041
H	-2.88989	3.96115	-2.78292
H	-1.13173	3.95311	-2.81841
B	-1.85001	-0.28339	0.40227
B	-0.81808	1.07139	1.10903
O	-3.23082	-0.33542	0.56569
O	-1.42627	2.07870	1.84744
B	0.78445	-1.45249	0.96125
B	-1.04559	-0.70583	-1.20947
O	1.50426	-2.47327	1.56649
O	-1.77443	-1.08230	-2.33194
C	1.83618	-2.48112	2.95806
C	-2.89195	-1.96853	-2.26324
H	1.44688	-3.41859	3.37773
H	-3.41242	-1.84595	-1.31127
H	1.35088	-1.65055	3.47107
H	-2.52045	-3.00022	-2.30945
C	3.35264	-2.42805	3.10038
C	-3.80558	-1.65841	-3.44257

H	3.77915	-3.19841	2.44561
H	-4.20190	-0.64346	-3.30435
H	3.70415	-1.46196	2.71683
H	-3.18915	-1.62908	-4.35028
B	0.55253	-1.49489	-0.75288
B	0.40580	0.21357	-1.41366
O	1.10970	-2.53347	-1.48553
O	0.84046	0.54432	-2.69222
C	0.88933	-2.72321	-2.88334
C	2.00800	1.34654	-2.90327
H	0.61927	-1.77993	-3.36352
H	2.66656	1.28025	-2.03619
H	0.04553	-3.41478	-3.00891
H	1.68895	2.39000	-3.00256
C	2.16219	-3.29683	-3.49552
C	2.70376	0.86009	-4.16827
H	2.92515	-2.50668	-3.51011
H	2.81593	-0.22909	-4.09253
H	1.95838	-3.55504	-4.54513
H	2.04777	1.04919	-5.02802
C	-0.88164	-4.21708	0.35258
H	-0.79333	-4.49991	-0.70406
H	0.13286	-4.11528	0.74616
C	-2.30073	-1.64478	3.30621
H	-2.66045	-2.13364	2.39878
H	-2.11081	-2.41762	4.05901
C	-1.11871	2.34106	3.21552
H	-1.02605	1.39834	3.76382
H	-0.14382	2.84578	3.27142
C	-3.32434	-0.62736	3.80749
H	-3.08491	-0.33619	4.83995
H	-3.22187	0.27348	3.19587
C	-4.04115	0.84554	0.56086
H	-4.34668	1.04653	1.59249
H	-3.46354	1.69985	0.21235
C	-5.25437	0.60314	-0.32692
H	-5.82008	-0.24729	0.07635
H	-4.89249	0.29835	-1.31667
C	-1.64764	-5.27238	1.14014
H	-1.04558	-6.19136	1.09684
H	-1.67494	-4.96565	2.19434
C	-4.77440	-1.12588	3.71984
H	-4.96705	-1.36676	2.66425
C	-5.00289	-2.39598	4.54972
H	-4.37234	-3.22527	4.21143
H	-4.77711	-2.21381	5.60868
H	-6.04593	-2.72634	4.48302
C	-5.74769	-0.02018	4.14521
H	-5.61274	0.88621	3.54392
H	-6.78937	-0.34414	4.03505
H	-5.59288	0.25217	5.19721

C	-2.20485	3.21893	3.81945
H	-1.96058	3.33128	4.88517
H	-3.16530	2.68632	3.77565
C	-2.36259	4.61849	3.19093
H	-1.35162	5.02900	3.03861
C	-3.10735	5.54845	4.15849
H	-3.22153	6.55301	3.73485
H	-4.11304	5.16146	4.36878
H	-2.57940	5.64166	5.11493
C	-3.07739	4.59314	1.83084
H	-3.18461	5.60985	1.43333
H	-2.54465	3.98332	1.09990
H	-4.08727	4.17598	1.94197
C	2.53309	4.98785	-1.16491
H	2.96406	3.98945	-1.31583
C	3.68466	5.97647	-0.95091
H	4.29106	5.69627	-0.08159
H	4.34437	6.01170	-1.82586
H	3.30384	6.99198	-0.78017
C	1.72311	5.35755	-2.41361
H	0.94940	4.61474	-2.63243
H	1.22701	6.32834	-2.28379
H	2.36862	5.42868	-3.29607
C	3.87358	-2.62795	4.53110
H	3.53047	-3.61373	4.88108
C	5.40758	-2.63205	4.52978
H	5.80708	-2.81166	5.53460
H	5.80455	-3.40745	3.86385
H	5.79552	-1.66503	4.18420
C	3.33737	-1.56609	5.50026
H	3.62598	-0.56222	5.16706
H	2.24538	-1.58661	5.57475
H	3.74450	-1.71478	6.50712
C	-6.18314	1.82265	-0.48370
H	-7.03623	1.48453	-1.08946
C	-5.50415	2.96913	-1.24857
H	-4.64509	3.37063	-0.70006
H	-5.14331	2.63050	-2.22703
H	-6.20543	3.79476	-1.41618
C	-6.74027	2.30918	0.86188
H	-7.19673	1.48725	1.42605
H	-5.95300	2.74654	1.48707
H	-7.50354	3.08129	0.71206
C	-2.02882	3.48812	-4.72754
H	-2.81878	2.81385	-5.09333
C	-2.35857	4.90713	-5.20554
H	-2.37370	4.96540	-6.30006
H	-3.33593	5.23631	-4.83426
H	-1.60629	5.62012	-4.84395
C	-0.68915	3.02055	-5.31812
H	0.12314	3.68362	-4.99186

H	-0.42985	2.00302	-5.00945
H	-0.71567	3.04221	-6.41367
C	4.08662	1.49276	-4.41692
H	4.42422	1.12469	-5.39617
C	4.02105	3.02463	-4.49410
H	3.25115	3.35736	-5.20067
H	3.78862	3.46107	-3.51635
H	4.98116	3.44171	-4.81904
C	5.12111	1.04108	-3.37512
H	4.86465	1.39903	-2.37182
H	5.18744	-0.05260	-3.32997
H	6.11695	1.42871	-3.61911
C	2.79305	1.37387	2.48149
H	2.76430	2.01882	1.60091
H	3.54608	0.60242	2.29046
C	3.12256	2.16483	3.73765
H	2.37713	2.96358	3.85240
H	3.00565	1.50371	4.60532
C	4.53715	2.77848	3.74176
H	4.63318	3.32803	4.68899
C	4.73512	3.78910	2.60210
H	5.70890	4.28578	2.68423
H	4.69476	3.30255	1.62053
H	3.96020	4.56448	2.62165
C	5.63984	1.70838	3.72208
H	5.49691	0.97393	4.52351
H	5.66028	1.16552	2.76980
H	6.62688	2.16523	3.85784
C	6.14727	-2.07194	-0.62005
H	6.05844	-2.11219	-1.71725
C	7.59288	-1.69440	-0.27734
H	8.30037	-2.43559	-0.66665
H	7.85934	-0.71745	-0.69705
H	7.73102	-1.64028	0.81025
C	5.80439	-3.46265	-0.06789
H	5.83809	-3.45998	1.02932
H	4.80538	-3.79217	-0.37077
H	6.52183	-4.21143	-0.42278
C	2.73037	-4.51950	-2.75595
H	2.87361	-4.22278	-1.70976
C	4.09476	-4.90800	-3.33551
H	4.53330	-5.75035	-2.78796
H	4.00675	-5.20419	-4.38908
H	4.80092	-4.07031	-3.28222
C	1.76183	-5.70794	-2.77614
H	0.81467	-5.46555	-2.28251
H	1.53760	-6.01625	-3.80597
H	2.19282	-6.57159	-2.25657
C	-3.08095	-5.60201	0.66764
H	-3.37620	-6.50866	1.21645
C	-4.10482	-4.51162	1.01761

H	-4.09845	-4.29779	2.09283
H	-3.88687	-3.57619	0.49727
H	-5.11783	-4.83503	0.74830
C	-3.12711	-5.93885	-0.82766
H	-2.40567	-6.72264	-1.08950
H	-4.12444	-6.28651	-1.11987
H	-2.89760	-5.05653	-1.43444
C	-4.97562	-2.64100	-3.64423
H	-5.60406	-2.20980	-4.43672
C	-4.50282	-4.01504	-4.13993
H	-3.89738	-3.92184	-5.04922
H	-3.89896	-4.53178	-3.38656
H	-5.35831	-4.66089	-4.36965
C	-5.84811	-2.77785	-2.38778
H	-6.73682	-3.38471	-2.59639
H	-5.30378	-3.26358	-1.57016
H	-6.18455	-1.79947	-2.02656

S9.8.2. $[1]^{\bullet+}$

	x	*y*	*z*
B	0.78606	0.37113	1.53885
O	1.49843	0.82486	2.62003
B	-0.62920	-0.65432	1.80585
O	-0.98219	-0.99268	3.08092
B	0.60545	1.31768	0.01413
O	1.18430	2.55337	-0.14484
C	0.45024	3.78403	-0.27309
H	-0.25460	3.86923	0.55941
H	-0.14015	3.74510	-1.19168
C	1.44054	4.93409	-0.27662
H	1.99518	4.91243	0.67003
H	0.86940	5.87306	-0.28626
B	1.59122	-0.13076	-0.05247
O	2.95534	-0.00735	-0.18002
C	3.80957	-1.13019	-0.46798
H	3.73825	-1.34982	-1.54009
H	3.44526	-2.00346	0.07515
C	5.23263	-0.76810	-0.08521
H	5.47218	0.20590	-0.52943
H	5.29256	-0.64223	1.00480
B	-0.88058	-1.81123	0.34389
B	-1.10505	0.92042	-0.69541
O	-1.48390	-3.03012	0.49810
O	-1.86548	1.85093	-1.35008
C	-2.08636	1.81445	-2.77591
H	-3.02027	1.26610	-2.94713
H	-1.27950	1.25814	-3.25070
C	-2.18245	3.23450	-3.30568
H	-3.05012	3.72708	-2.85104
H	-1.29645	3.79661	-2.98253
B	-1.86330	-0.36143	0.42565
B	-0.90619	1.04183	1.04849
O	-3.22381	-0.49259	0.56041
O	-1.55177	2.02607	1.75034
B	0.83097	-1.42304	1.05461
B	-1.04036	-0.86108	-1.18145
O	1.60168	-2.36391	1.68040
O	-1.75198	-1.27214	-2.27976
C	1.95739	-2.34892	3.07634
C	-2.78250	-2.27445	-2.22446
H	1.68447	-3.33200	3.47692
H	-3.32905	-2.17430	-1.28500
H	1.38006	-1.58617	3.59850
H	-2.30030	-3.25844	-2.23099
C	3.45884	-2.12031	3.19046
C	-3.68756	-2.08720	-3.43141
H	3.95822	-2.82599	2.51565
H	-4.15675	-1.09743	-3.35384

H	3.68863	-1.11273	2.82152
H	-3.06124	-2.06847	-4.33217
B	0.63251	-1.54109	-0.68494
B	0.37359	0.15739	-1.43176
O	1.26000	-2.54143	-1.37335
O	0.77178	0.46113	-2.70445
C	0.95457	-2.96312	-2.71128
C	1.99374	1.16087	-3.01543
H	0.56202	-2.11769	-3.28398
H	2.69938	1.04443	-2.19199
H	0.17229	-3.72939	-2.65683
H	1.74180	2.22235	-3.09849
C	2.23046	-3.51031	-3.33326
C	2.54454	0.61601	-4.32440
H	2.92418	-2.67292	-3.48890
H	2.58033	-0.47839	-4.25086
H	1.98468	-3.90281	-4.32991
H	1.83863	0.85654	-5.12908
C	-0.80446	-4.28376	0.67529
H	-0.71145	-4.74539	-0.31499
H	0.20317	-4.10877	1.05915
C	-2.28972	-1.48202	3.43720
H	-2.73472	-1.98814	2.57797
H	-2.12343	-2.21536	4.23011
C	-1.07057	2.61235	2.96944
H	-0.85206	1.80779	3.68019
H	-0.12877	3.13686	2.76252
C	-3.17645	-0.33529	3.91148
H	-2.81099	0.03336	4.87914
H	-3.07387	0.49024	3.20002
C	-4.13279	0.62490	0.54229
H	-4.55337	0.71181	1.54641
H	-3.59124	1.54215	0.31774
C	-5.22479	0.34783	-0.48150
H	-5.76456	-0.55706	-0.17524
H	-4.74506	0.12027	-1.44179
C	-1.59555	-5.17747	1.62008
H	-1.01720	-6.10727	1.71084
H	-1.60230	-4.71706	2.61688
C	-4.66044	-0.72297	4.02025
H	-4.98229	-1.06719	3.02574
C	-4.89246	-1.86813	5.01446
H	-4.38009	-2.78803	4.71111
H	-4.53142	-1.59552	6.01419
H	-5.95943	-2.10063	5.09794
C	-5.49774	0.50562	4.39596
H	-5.35950	1.32281	3.67745
H	-6.56530	0.26215	4.42487
H	-5.21456	0.88208	5.38666
C	-2.11277	3.56803	3.52278
H	-1.74750	3.88338	4.50954

H	-3.04611	3.01635	3.70047
C	-2.40284	4.82234	2.67419
H	-1.43346	5.25158	2.37349
C	-3.13489	5.86678	3.52779
H	-3.33398	6.77715	2.95225
H	-4.09992	5.47582	3.87443
H	-2.55029	6.14605	4.41159
C	-3.21124	4.52238	1.40202
H	-3.44467	5.45153	0.86964
H	-2.68275	3.85702	0.71625
H	-4.16488	4.04434	1.66179
C	2.43146	4.92070	-1.45374
H	2.89769	3.92583	-1.47810
C	3.53758	5.95789	-1.22947
H	4.07437	5.76978	-0.29252
H	4.26737	5.93991	-2.04640
H	3.12018	6.97136	-1.17872
C	1.72602	5.16066	-2.79516
H	0.97315	4.39426	-3.01286
H	1.21869	6.13359	-2.79919
H	2.44361	5.15704	-3.62214
C	4.02393	-2.28719	4.60997
H	3.79540	-3.31006	4.94477
C	5.54909	-2.12677	4.57827
H	5.98348	-2.27687	5.57241
H	6.01371	-2.84710	3.89498
H	5.82570	-1.11903	4.24203
C	3.39699	-1.30648	5.60925
H	3.58401	-0.27087	5.30039
H	2.31323	-1.43699	5.69902
H	3.82980	-1.43883	6.60660
C	-6.21540	1.51449	-0.67029
H	-7.01874	1.13141	-1.31426
C	-5.57121	2.70269	-1.39942
H	-4.73991	3.12995	-0.82751
H	-5.18311	2.39956	-2.37898
H	-6.30314	3.50098	-1.56321
C	-6.85588	1.95545	0.65374
H	-7.27384	1.10296	1.20210
H	-6.12799	2.45121	1.30779
H	-7.66687	2.66876	0.47331
C	-2.27487	3.29902	-4.84077
H	-3.09001	2.63361	-5.16371
C	-2.62132	4.72455	-5.28652
H	-2.70874	4.78714	-6.37646
H	-3.56902	5.06003	-4.85083
H	-1.83996	5.42887	-4.97363
C	-0.97503	2.82657	-5.51101
H	-0.13269	3.45994	-5.20204
H	-0.72428	1.79018	-5.26025
H	-1.05473	2.89190	-6.60134

C	3.94800	1.14627	-4.68063
H	4.17403	0.75900	-5.68307
C	3.98982	2.67919	-4.75279
H	3.19547	3.07225	-5.39822
H	3.87066	3.12947	-3.75987
H	4.94923	3.02370	-5.15296
C	5.02659	0.61089	-3.72725
H	4.89420	0.99549	-2.70919
H	5.00832	-0.48470	-3.67865
H	6.02503	0.91299	-4.06097
C	2.67875	1.63934	2.47472
H	2.55504	2.31054	1.62386
H	3.51054	0.96665	2.24245
C	2.91624	2.39968	3.76734
H	2.07933	3.09282	3.92580
H	2.89510	1.68737	4.60053
C	4.24419	3.18394	3.78745
H	4.27509	3.70484	4.75381
C	4.30334	4.25259	2.68547
H	5.19584	4.87762	2.79669
H	4.34302	3.80188	1.68619
H	3.42740	4.91161	2.72290
C	5.46852	2.25808	3.72671
H	5.42307	1.48544	4.50326
H	5.55163	1.75548	2.75532
H	6.39205	2.82756	3.87586
C	6.26703	-1.81027	-0.54295
H	6.18045	-1.90701	-1.63636
C	7.68398	-1.32164	-0.22193
H	8.43680	-2.03208	-0.57989
H	7.88654	-0.35063	-0.68783
H	7.81976	-1.20937	0.86120
C	6.01524	-3.19204	0.07689
H	6.04784	-3.13527	1.17265
H	5.04286	-3.60669	-0.21025
H	6.78277	-3.90560	-0.24132
C	2.93288	-4.59603	-2.49961
H	3.11479	-4.17287	-1.50327
C	4.28874	-4.94669	-3.12195
H	4.82186	-5.68605	-2.51444
H	4.16515	-5.36782	-4.12752
H	4.92810	-4.05953	-3.20723
C	2.06176	-5.84612	-2.32733
H	1.12766	-5.62401	-1.79860
H	1.80369	-6.28411	-3.29990
H	2.59081	-6.61110	-1.74879
C	-3.04248	-5.52908	1.20360
H	-3.33465	-6.37812	1.83700
C	-4.04845	-4.40089	1.47920
H	-4.02246	-4.09992	2.53349
H	-3.83997	-3.51464	0.87380

H	-5.06826	-4.73623	1.25781
C	-3.12590	-5.99581	-0.25476
H	-2.41374	-6.80251	-0.46604
H	-4.12979	-6.36627	-0.48745
H	-2.91581	-5.17001	-0.94369
C	-4.78244	-3.16246	-3.58244
H	-5.40461	-2.84088	-4.42865
C	-4.20252	-4.53794	-3.94122
H	-3.56469	-4.48140	-4.83092
H	-3.60433	-4.95464	-3.12296
H	-5.00546	-5.25311	-4.14985
C	-5.69176	-3.24700	-2.34746
H	-6.53547	-3.91985	-2.53450
H	-5.15469	-3.63364	-1.47331
H	-6.09866	-2.26412	-2.08259

S10. References

(1) Wixtrom, A. I.; Shao, Y.; Jung, D.; Machan, C. W.; Kevork, S. N.; Qian, E. A.; Axtell, J. C.; Khan, S. I.; Kubiak, C. P.; Spokoyny, A. M. Rapid Synthesis of Redox-Active Dodecaborane $B_{12}(OR)_{12}$ Clusters Under Ambient Conditions. *Inorg. Chem. Front.* **2016**, *3*, 711–717.

(2) Yueh, W.; Bauld, N. L. Mechanistic Criteria for Cation Radical Reactions: Aminium Salt-Catalyzed Cyclopropanation. *J. Am. Chem. Soc.* **1995**, *117* (21), 5671–5676.

(3) Farha, O. K.; Julius, R. L.; Lee, M. W.; Huertas, R. E.; Knobler, C. B.; Hawthorne, M. F. Synthesis of Stable Dodecaalkoxy Derivatives of Hypercloso-$B_{12}H_{12}$. *J. Am. Chem. Soc.* **2005**, *127* (51), 18243–18251.

(4) Bard, A. J.; Faulkner, L. R. *Electrochemical Methods*, 2nd ed.; John Wiley & Sons, 2001.

(5) Connelly, N. G.; Geiger, W. E. Chemical Redox Agents for Organometallic Chemistry. *Chem. Rev.* **1996**, *96* (2), 877–910.

(6) Frisch, M. J.; Trucks, G. W.; Schlegel, H. B.; Scuseria, G. E.; Robb, M. A.; Cheeseman, J. R.; Scalmani, G.; Barone, V.; Petersson, G. A.; Nakatsuji, H.; X. Li, M. C.; Marenich, A. V.; Bloino, J.; Janesko, B. G.; Gomperts, R.; Mennucci, B.; Hratchian, H. P.; Ortiz, J. V.; Izmaylov, A. F.; Sonnenberg, J. L.; Williams-Young, D.; Ding, F.; Lipparini, F.; Egidi, F.; Goings, J.; Peng, B.; Petrone, A.; Henderson, T.; Ranasinghe, D.; Zakrzewski, V. G.; Gao, J.; Rega, N.; Zheng, G.; Liang, W.; Hada, M.; Ehara, M.; Toyota, K.; Fukuda, R.; Hasegawa, J.; Ishida, M.; Nakajima, T.; Honda, Y.; Kitao, O.; Nakai, H.; Vreven, T.; Throssell, K.; J. A. Montgomery, J.; Peralta, J. E.; Ogliaro, F.; Bearpark, M. J.; Heyd, J. J.; Brothers, E. N.; Kudin, K. N.; Staroverov, V. N.; Keith, T. A.; Kobayashi, R.; Normand, J.; Raghavachari, K.; Rendell, A. P.; Burant, J. C.; Iyengar, S. S.; Tomasi, J.; Cossi, M.; Millam, J. M.; Klene, M.; Adamo, C.; Cammi, R.; Ochterski, J. W.; Martin, R. L.; Morokuma, K.; Farkas, O.; Foresman, J. B.; Fox, D. J. *Gaussian 16, Revision C.01*; Gaussian, Inc.: Wallingford, CT, 2016.

(7) Becke, A. D. Density-Functional Thermochemistry. III. The Role of Exact Exchange. *J. Chem. Phys.* **1993**, *98* (7), 5648–5652.

(8) Lee, C.; Yang, W.; Parr, R. G. Development of the Colle-Salvetti Correlation-Energy Formula into a Functional of the Electron Density. *Phys. Rev. B* **1988**, *37* (2), 785–789.

(9) Vosko, S. H.; Wilk, L.; Nusair, M. Accurate Spin-Dependent Electron Liquid Correlation Energies for Local Spin Density Calculations: A Critical Analysis. *Can. J. Phys.* **1980**, *58* (8), 1200–1211.

(10) Stephens, P. J.; Devlin, F. J.; Chabalowski, C. F.; Frisch, M. J. Ab Initio Calculation of Vibrational Absorption and Circular Dichroism Spectra Using Density Functional Force Fields. *J. Phys. Chem.* **1994**, *98* (45), 11623–11627.

(11) Grimme, S.; Ehrlich, S.; Goerigk, L. Effect of the Damping Function in Dispersion Corrected Density Functional Theory. *J. Comput. Chem.* **2011**, *32* (7), 1456–1465.

(12) Yanai, T.; Tew, D. P.; Handy, N. C. A New Hybrid Exchange–Correlation Functional

Using the Coulomb-Attenuating Method (CAM-B3LYP). *Chem. Phys. Lett.* **2004**, *393* (1–3), 51–57.

(13) Ditchfield, R.; Hehre, W. J.; Pople, J. A. Self-Consistent Molecular-Orbital Methods. IX. An Extended Gaussian-Type Basis for Molecular-Orbital Studies of Organic Molecules. *J. Chem. Phys.* **1971**, *54* (2), 724–728.

(14) Grimme, S. Supramolecular Binding Thermodynamics by Dispersion-Corrected Density Functional Theory. *Chem. - A Eur. J.* **2012**, *18* (32), 9955–9964.

(15) Funes-Ardoiz, I.; Paton, R. S. GoodVibes v1.0.1. https://doi.org/10.5281/zenodo.56091.

(16) Peach, M. J. G.; Benfield, P.; Helgaker, T.; Tozer, D. J. Excitation Energies in Density Functional Theory: An Evaluation and a Diagnostic Test. *J. Chem. Phys.* **2008**, *128* (4), 044118.

(17) Jacquemin, D.; Wathelet, V.; Perpète, E. A.; Adamo, C. Extensive TD-DFT Benchmark: Singlet-Excited States of Organic Molecules. *J. Chem. Theory Comput.* **2009**, *5* (9), 2420–2435.

(18) Marenich, A. V.; Cramer, C. J.; Truhlar, D. G. Universal Solvation Model Based on Solute Electron Density and on a Continuum Model of the Solvent Defined by the Bulk Dielectric Constant and Atomic Surface Tensions. *J. Phys. Chem. B* **2009**, *113* (18), 6378–6396.

(19) Gaussian. Creating UV/Visible Plots from the Results of Excited States Calculations https://gaussian.com/uvvisplot/.

(20) Schäfer, A.; Horn, H.; Ahlrichs, R. Fully Optimized Contracted Gaussian Basis Sets for Atoms Li to Kr. *J. Chem. Phys.* **1992**, *97* (4), 2571–2577.

(21) Schäfer, A.; Huber, C.; Ahlrichs, R. Fully Optimized Contracted Gaussian Basis Sets of Triple Zeta Valence Quality for Atoms Li to Kr. *J. Chem. Phys.* **1994**, *100* (8), 5829–5835.

(22) Weigend, F.; Ahlrichs, R. Balanced Basis Sets of Split Valence, Triple Zeta Valence and Quadruple Zeta Valence Quality for H to Rn: Design and Assessment of Accuracy. *Phys. Chem. Chem. Phys.* **2005**, *7* (18), 3297–3305.

(23) Cheeseman, J. R. A Comparison of Models for Calculating Nuclear Magnetic Resonance Shielding Tensors. *J. Chem. Phys.* **1996**, *104* (14), 5497–5509.

(24) Vasiliu, M.; Arduengo, A. J.; Dixon, D. A. Computational Studies of the Properties of Azole· x BH 3 Adducts for Chemical Hydrogen Storage Systems. *J. Phys. Chem. C* **2012**, *116* (42), 22196–22211.

(25) Haberecht, M. C.; Heilmann, J. B.; Haghiri, A.; Bolte, M.; Bats, J. W.; Lerner, H. W.; Holthausen, M. C.; Wagner, M. Multiply Borylated Arenes: X-Ray Crystal Structure Analyses and Quantum Chemical Calculations. *Zeitschrift fur Anorg. und Allg. Chemie* **2004**, *630* (6), 904–913.

(26) Schrödinger, L. *The PyMOL Molecular Graphics Development Component, Version 1.8*; 2015.

(27) Lee, C.; Yang, W.; Parr, R. G. Development of the Colle-Salvetti Correlation-Energy Formula into a Functional of the Electron Density. *Phys. Rev. B* **1988**, *37*, 785–789.

(28) Grimme, S.; Ehrlich, S.; Goerigk, L. Effect of the Damping Function in Dispersion Corrected Density Functional Theory. *J. Comput. Chem.* **2011**, *32* (7), 1456–1465.

(29) Peymann, T.; Knobler, C. B.; Khan, S. I.; Hawthorne, M. F. Dodeca(Benzyloxy)Dodecaborane, $B_{12}(OCH_2Ph)_{12}$: A Stable Derivative of Hypercloso-$B_{12}H_{12}$. *Angew. Chem. - Int. Ed.* **2001**, *40*, 1664–1667.

(30) Ho, J. Are Thermodynamic Cycles Necessary for Continuum Solvent Calculation of PKa's and Reduction Potentials? *Phys. Chem. Chem. Phys.* **2015**, *17* (4), 2859–2868.

(31) Marenich, A. V.; Ho, J.; Coote, M. L.; Cramer, C. J.; Truhlar, D. G. Computational Electrochemistry: Prediction of Liquid-Phase Reduction Potentials. *Phys. Chem. Chem. Phys.* **2014**, *16* (29), 15068–15106.

(32) Ree, N.; Andersen, C. L.; Kilde, M. D.; Hammerich, O.; Nielsen, M. B.; Mikkelsen, K. V. The Quest for Determining One-Electron Redox Potentials of Azulene-1-Carbonitriles by Calculation. *Phys. Chem. Chem. Phys.* **2018**, *20* (11), 7438–7446.